



TALLINN UNIVERSITY OF TECHNOLOGY  
SCHOOL OF ENGINEERING  
Department of Energy Technology

**THERMAL ENERGY HARVESTING BY MEANS OF  
THERMOELECTRICS FOR AN EXHAUST GAS  
CLEANING SYSTEM ON BOARD OF A VESSEL**

**JÄÄKSOOJUSE KASUTAMINE LAEVAL SUITSUGAASIDE  
PESURILE INTEGREERITUD TERMoeLEKTRILISE  
SEADMEGA**

MASTER THESIS

Student: Karl Mustjõgi

Student code: 182965

Supervisor: Eduard Latõšov, Associate Professor

Co-supervisor: Dmitri Nešumajev, Senior Research Scientist

Tallinn 2020



## **Non-exclusive Licence for Publication and Reproduction of Graduation Thesis<sup>1</sup>**

I, Karl Mustjõgi, (date of birth: 04.01.1995) hereby

1. grant Tallinn University of Technology (TalTech) a non-exclusive license for my thesis Thermal energy harvesting by means of thermoelectrics for an exhaust gas cleaning system on board of a vessel,

supervised by

Eduard Latõšov and Dmitri Nešumajev,

1.1 reproduced for the purposes of preservation and electronic publication, incl. to be entered in the digital collection of TalTech library until expiry of the term of copyright;

1.2 published via the web of TalTech, incl. to be entered in the digital collection of TalTech library until expiry of the term of copyright.

1.3 I am aware that the author also retains the rights specified in clause 1 of this license.

2. I confirm that granting the non-exclusive license does not infringe third persons' intellectual property rights, the rights arising from the Personal Data Protection Act or rights arising from other legislation.

---

<sup>1</sup> *Non-exclusive Licence for Publication and Reproduction of Graduation Thesis is not valid during the validity period of restriction on access, except the university`s right to reproduce the thesis only for preservation purposes.*

\_\_\_\_\_ (signature)

\_\_\_\_\_ (date)

**Department of Energy Technology**

**THESIS TASK**

**Student:** Karl Mustjõgi, 182965

Study programme, main speciality: MASM02/18, Energy Technology and Thermal Engineering

Supervisor(s): Associate Professor, Eduard Latõšov, 620 3908

Senior Research Scientist, Dmitri Nešumajev, 620 3910

**Thesis topic:**

Thermal energy harvesting by means of thermoelectrics for an exhaust gas cleaning system on board of a vessel

Jäaksoojuse kasutamine laeval suitsugaaside pesurile integreeritud termoelektrilise seadmega

**Thesis main objectives:**

1. Calculate the rate of heat exchange for quenching
2. Evaluate the possibility of integrating thermoelectric generator system to wet scrubber
3. Evaluate the economic sustainability of the integration

**Thesis tasks and time schedule:**

| No | Task description   | Deadline |
|----|--|----------|
| 1. | Collecting input information                                 | 03.2020  |
| 2. | Give an overview of thermoelectric materials and generators  | 04.2020  |
| 3. | Give an overview of exhaust gas cleaning systems in maritime | 04.2020  |
| 4. | Give a detailed overview of the investigated case            | 04.2020  |
| 5. | Calculate the properties of heat exchanger                   | 05.2020  |
| 6. | Evaluate the economic sustainability of the integration      | 05.2020  |

**Language:** English **Deadline for submission of thesis:** ".....".....2020.a

**Student:** Karl Mustjõgi ..... ".....".....2020.a  
/signature/

**Supervisor:** Eduard Latõšov ..... ".....".....2020.a  
/signature/

**Co-supervisor:** Dmitri Nešumajev ..... ".....".....2020.a  
/signature/

**Head of study programme:**

Eduard Latšov

.....".....".....2020.a

*/signature/*

*The author requests to not publish the contents of this thesis due to the usage of confidential information of the company.*

## CONTENTS

|   |    |
|---|----|
| PREFACE .....   | 8  |
| INTRODUCTION.....   | 9  |
| 1. REVIEW OF THERMOELECTRIC MATERIALS .....   | 11 |
| 1.1 Seebeck coefficient .....   | 13 |
| 1.2 SnSe.....   | 13 |
| 1.3 PbTe .....  | 14 |
| 1.4 Bi <sub>2</sub> Te <sub>3</sub> .....   | 14 |
| 1.5 SiGe.....   | 14 |
| 1.6 Cu <sub>2</sub> Se.....   | 14 |
| 1.7 Skutterudites .....   | 15 |
| 1.8 Other thermoelectric materials .....  | 15 |
| 2. REVIEW OF THERMOELECTRIC GENERATORS .....  | 16 |
| 2.1 Thermoelectric generator working principles.....  | 16 |
| 2.2 Thermoelectric generators applications.....   | 17 |
| 2.2.1 Electricity generation in extreme environments .....                                    | 17 |
| 2.2.2 Waste heat recovery applications.....   | 17 |
| 2.2.3 Decentralized domestic power and CHP generation systems.....                            | 18 |
| 2.2.4 Micro-generation for sensors and microelectronics .....                                 | 18 |
| 2.2.5 Solar thermoelectric generators.....  | 19 |
| 3. EXHAUST GAS CLEANING SYSTEMS IN MARITIME.....  | 20 |
| 3.1 Wet scrubbers.....  | 20 |
| 3.1.1 Wet scrubber working principle.....   | 20 |
| 3.1.2 Workflow of wet scrubbers.....  | 22 |
| 3.2 Dry scrubbers.....  | 23 |
| 3.3 Selective catalytic reduction (SCR).....  | 23 |
| 3.4 Exhaust gas recirculation (EGR).....  | 24 |
| 4. CASE DESCRIPTION .....   | 26 |
| 5. METHOD TO EVALUATE THE POSSIBILITY OF REPLACING QUENCHING SEGMENT<br>WITH TEG SYSTEM ..... | 37 |
| 5.1 The rate of heat exchange .....   | 37 |
| 5.2 Properties of the heat exchanger .....  | 38 |
| 5.3 Overall thermal resistance .....  | 39 |
| 6. QUENCHING SEGMENT REPLACEMENT EVALUATION.....  | 46 |
| 6.1 Rate of heat exchange from exhaust gas .....  | 46 |
| 6.2 Heat exchanger evaluation.....  | 46 |
| 6.2.1 Thermal resistance of exhaust gas .....   | 46 |

|   |    |
|---|----|
| 6.2.2 Thermal resistance of tubes in heat exchanger .....                       | 48 |
| 6.2.3 Thermal resistance of water in heat exchanger .....                       | 48 |
| 6.2.4 Exhaust gas temperature at the outlet of heat exchanger .....             | 49 |
| 6.3 Optimising the heat exchanger .....   | 50 |
| 6.4 Properties of TEG system .....  | 54 |
| 7. Economic evaluation of replacing quenching segment with TEG SYSTEM .....     | 55 |
| 7.1 Power gain on integrating TEG system .....                                  | 55 |
| 7.2 Reduced cost of building the wet scrubber compared to current version ..... | 56 |
| 7.3 Financial calculations .....  | 56 |
| SUMMARY .....   | 58 |
| KOKKUVÕTE .....   | 60 |
| LIST OF REFERENCES .....  | 62 |
| Appendix 1 Exhaust gas average isobaric specific heat calculation .....         | 65 |
| Appendix 2 Part list and prices of quenching segment .....                      | 66 |

## **PREFACE**

The thesis topic was initiated by Vasileios Besikiotis, the manager of research and development department at Clean Marine AS, based on the ongoing research project at the company which is investigated in this study. The company designs exhaust gas cleaning systems for maritime applications and is located in Norway. The information was obtained from previous projects with the company, through information inquiries and literature.

The author of this thesis would like to thank his supervisors Eduard Latõšov and Dmitri Nešumajev, and the consultant of the company Vasileios Besikiotis.

The wet scrubbers investigated have a quenching segment which is used to cool the exhaust gas before scrubbing. The segment is expensive to manufacture relative to its mass compared to the rest of the scrubber. For this reason, the integration of thermoelectric system is considered by replacing quenching segment with heat exchanger that would provide heat to the thermoelectric generator. The possibility of doing that is evaluated by comparing the needed exhaust gas outlet temperature from heat exchanger to the exhaust gas outlet temperatures that heat exchanger could provide. The economic evaluation is given based on the results.

Keywords: exhaust gas cleaning system, wet scrubber, thermoelectric generator, heat exchanger, master thesis



## INTRODUCTION

From the year 1965 to 2017 global waste heat is estimated to be about 80% of the consumed global energy with industry contributing 44%, commercial and residential contributing 36%, and transportation 20% to the total waste heat [1]. More optimistic study found that the quantity of waste heat accounts for 49,3-53,0% of the global input energy [2]. In addition, maritime sector contributes to about 2,7% of the global CO<sub>2</sub> emissions and is estimated to raise up to 19% in the future if appropriate measures are not taken [3]. One of the solutions to decrease both numbers is through waste heat recovery systems on vessels. As some of the waste heat is turned into useful energy, the primary fuel consumption and therefore the CO<sub>2</sub> emissions are reduced.

This study aims to harvest the heat from the exhaust gas of a cargo vessel that is using slow speed 2-stroke diesel engine. Since wet scrubbers are used on many ships to clean the exhaust gas from particulate matter and sulphur oxides (SO<sub>x</sub>), the exhaust gas temperature must be decreased before scrubbing operation [4]. This rapid temperature lowering process is called quenching and is built into wet scrubbers. As the exhaust gas temperature must be decreased in any such case, the possibility of using that heat for electricity generation is investigated. This is driven by the high cost of material to manufacture quenching segment. For this study, the option is chosen to be thermoelectric generator (TEG) due to its ability of generating electricity directly from heat, low maintenance costs, and the absence of moving parts within that system [5]. This also means that replacing quenching in wet scrubbers might be a possibility. In order to evaluate that possibility, the properties of heat exchanger that provides TEG with hot water must be investigated. For this application, the heat exchanger would ideally replace the quenching segment and otherwise cost of manufacturing would turn into an investment. The investment period could be 10-20 years as the TEG systems are very durable and are regularly used in spacecrafts [6].

Thermoelectric generators were first introduced in the second half of the 19<sup>th</sup> century and their rapid development started with the discovery of semiconductor technology. From that point thermoelectric generators have been developed but not as much to be an attractive investment due to their low efficiency of under 3 % [6], [7]. In recent years, the enhancement of materials used in TEGs and increased efficiency have made the TEG systems a more competitive option for electricity generation in recovering waste heat applications [6].

The study contains an overview of thermoelectric materials, generators, and their applications. An overview is given on the exhaust gas cleaning systems and more precise look on the case at hand. A comparison is done between needed exhaust gas outlet temperature from heat exchanger to the heat exchanger's ability to do so. Thus, concluding whether the whole quenching segment could be replaced by a heat exchanger, half of that or the TEG system is added to the current version of a scrubber. In further discussion the payback time, net present value (NPV) and internal rate of interest (IRR) for an investment into integrating the TEG system to the scrubber is done to evaluate the economic sustainability.

# 1. REVIEW OF THERMOELECTRIC MATERIALS

Thermoelectric materials and devices made from them use direct conversion of temperature difference to electricity. The difference in temperatures can be obtained from solar panels, waste heat or any other heat source. The major advantage of using thermoelectric devices is the solid state in which the devices operate, meaning they have no moving parts. That in turn means the mentioned devices produce no noise or vibration [5]. The dimensionless thermoelectric figure of merit ( $ZT$ ) is the main value in comparing efficiencies of different materials with thermoelectric properties and is shown in equation (1.1) below [8].

$$ZT = \frac{\alpha^2 \sigma}{\kappa} T, \quad (1.1)$$

where  $ZT$  – thermoelectric figure of merit,

$\alpha$  – Seebeck coefficient, V/K,

$\sigma$  – electrical conductivity, S/m,

$\kappa$  – thermal conductivity of thermoelectric material, W/(m · K),

$T$  – temperature, K.

The component  $\alpha^2 \sigma$  of  $ZT$  is also referred to as the power factor or thermopower [5], [8]. As seen from the equation (1.1) for the  $ZT$  to be highest, Seebeck coefficient and electrical conductivity would need to be as high as possible but thermal conductivity inversely as low as possible. This creates the largest potential difference across the junction where electrical power is extracted from the device. The high Seebeck coefficient ensures a large potential, the high electrical conductivity minimizes the Joule heating effect and the low thermal conductivity is needed to create a large difference in temperature at opposite ends of the material [5]. The below figure (Figure 1.1) shows the most common classes of materials that have been researched with thermoelectric aim [5].

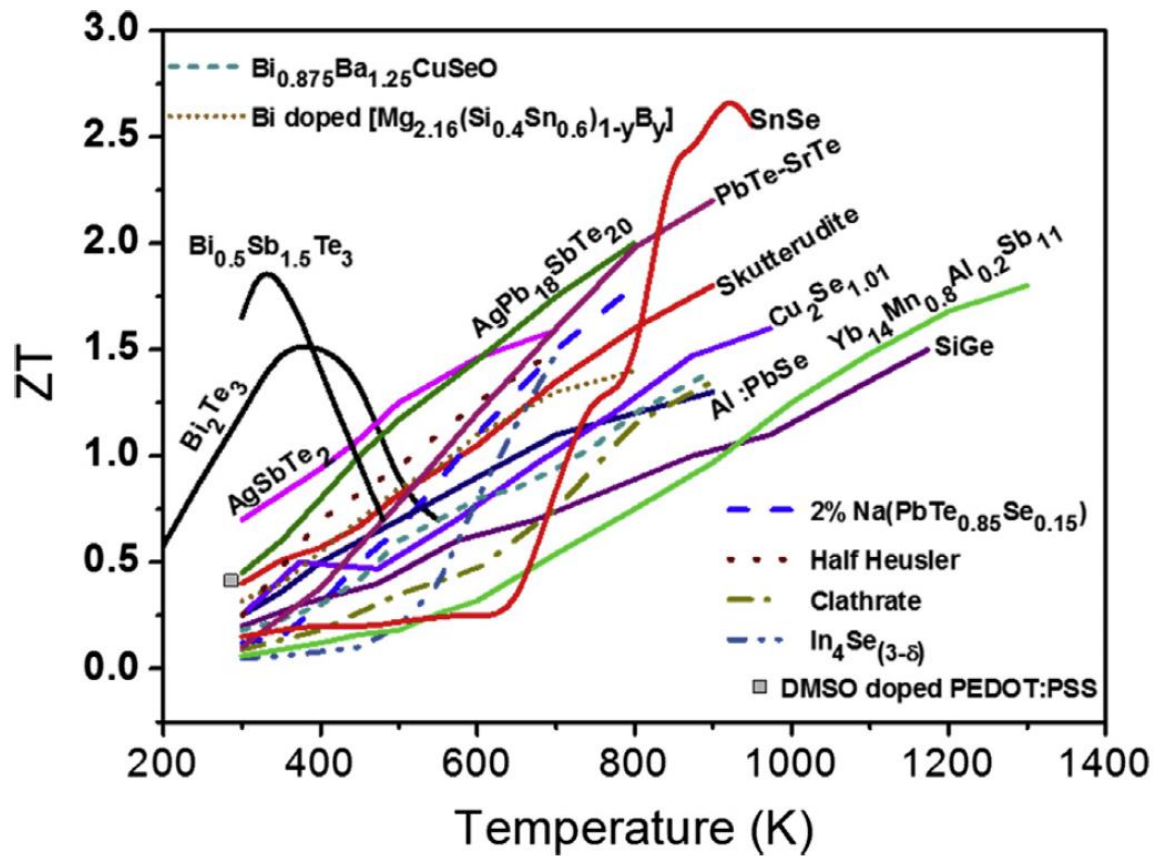


Figure 1.1 ZT values of different classes of materials over a range of temperatures: PbTe-SrTe, AgPb<sub>18</sub>SbTe<sub>20</sub>, 2% Na-doped PbTe<sub>0.82</sub>Se<sub>0.15</sub>, Ti<sub>x</sub>(Zr<sub>0.5</sub>Hf<sub>0.1</sub>)<sub>1-x</sub>NiSn half.Heusler alloy, Al-doped PbSe, Cu<sub>2</sub>Se<sub>1.01</sub>, Ba<sub>8</sub>Ga<sub>16</sub>Ge<sub>30</sub> (clathrates), Ba<sub>0.08</sub>Yb<sub>0.04</sub>La<sub>0.05</sub>Co<sub>4</sub>Sb<sub>12</sub> (skutterudites), melt-spun + spark plasma-sintered (SPS) Bi<sub>2</sub>Te<sub>3</sub>, AgSbTe<sub>2</sub>, SiGe, In<sub>4</sub>Se<sub>3-δ</sub> Yb<sub>14</sub>Mn<sub>0.8</sub>Al<sub>0.2</sub>Sb<sub>11</sub>, Bi<sub>0.875</sub>Ba<sub>1.25</sub>CuSeO, Bi-doped Mg<sub>2.16</sub>(Si<sub>0.4</sub>Sn<sub>0.6</sub>)<sub>1-y</sub>By, SnSe, Bi<sub>0.5</sub>Sb<sub>1.5</sub>Te<sub>3</sub> [5].

Historically the ZT values before 1990 were achieved up to 1,0 (Figure 1.2). The values of ZT were enhanced up to 1,7 in the period from 1990 to early 2010s by nanostructuring the formerly researched materials. Since the early 2010s many promising materials have been researched that show high ZT values. Furthermore, many of those materials are low-cost, earth-abundant and have low thermal conductivity [9].

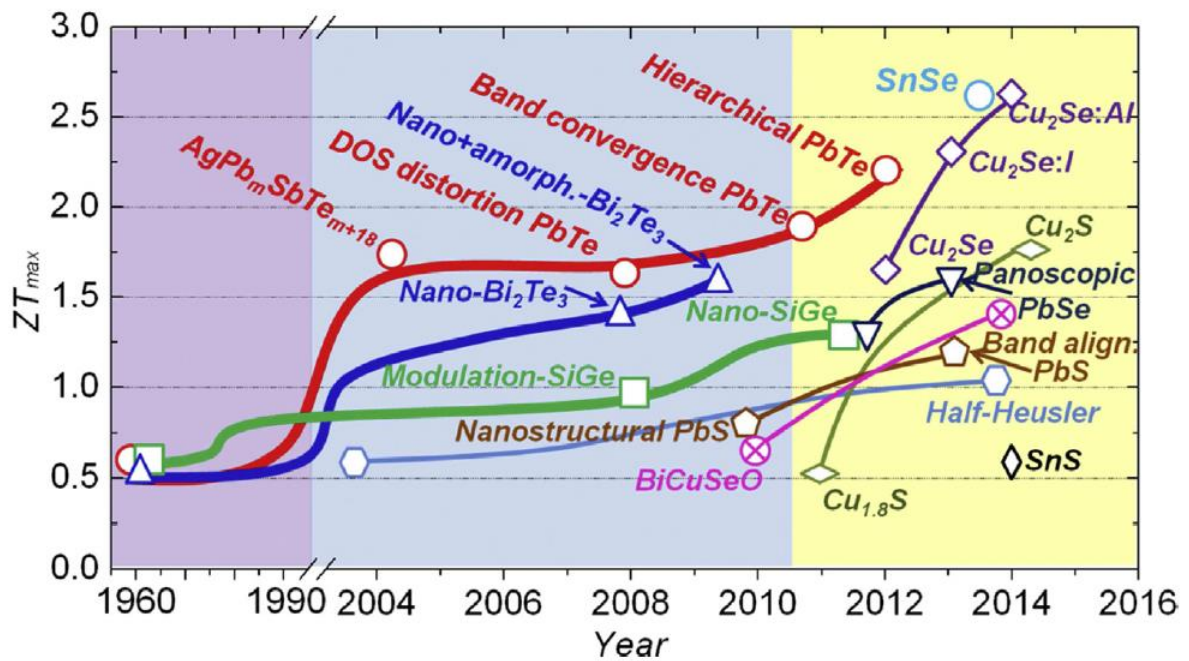


Figure 1.2 ZT values of thermoelectric materials over the years since 1960 [9]

## 1.1 Seebeck coefficient

The Seebeck coefficient is derived from the Seebeck effect which occurs in a material that has a different temperature between two points. Due to the temperature gradient electrons or electron holes from the hot side of the material travel towards the cold side. This leaves the hot side with more positive ions than negative and potential difference between hot and cold side can be measured. The magnitude of the voltage created per unit temperature difference in the material is the Seebeck coefficient [10].

## 1.2 SnSe

SnSe (Tin(II)Selenide) is mostly known as a semiconductor with a room temperature electrical resistivity between  $1-10\,000\ \Omega \cdot \text{m}$ . Given the high resistivity it has not been considered for use in thermoelectric devices but mostly in solar cells and electronic devices. The very low thermal conductivity compared to other crystalline materials of lower than  $0,4\ \text{W}/(\text{m} \cdot \text{K})$  at  $923\ \text{K}$  has brought scientists' attention to this material. The low thermal conductivity gives SnSe high ZTs of over 2,3 at temperatures  $723-973\ \text{K}$ . Possibly SnSe can be used in the temperature range of  $300 - 773\ \text{K}$ . As SnSe for applications in thermoelectric devices has only been considered since 2014 further research needs to be conducted for SnSe to be commercially available [8].

### 1.3 PbTe

PbTe (Lead telluride) is one of the most widely used material that thermoelectric semiconductor materials are based on. Its  $ZT$  value has been improved over the years to reach over 2,0 (Figure 1.2). PbTe has a maximum operating temperature of 900 K, has a high melting point and good chemical strength to go along with high figure of merit [11]. The thermal conductivity of  $2,3 \text{ W}/(\text{m} \cdot \text{K})$  and Seebeck coefficient of  $500 \mu\text{V}/\text{K}$  at room temperature makes PbTe a promising material for use in the temperature range of 600 – 800 K [5]. The Seebeck coefficient of PbTe based materials are enhanced by doping. Some of the doping agents used are  $\text{Bi}_2\text{Te}_3$ ,  $\text{TaTe}_2$ ,  $\text{MnTe}_2$ ,  $\text{Na}_2\text{Te}$ ,  $\text{K}_2\text{Te}$  and  $\text{Ag}_2\text{Te}$ . The doping agents substitute Pb or Te atoms and thus create additional positive or negative holes in the material to enhance the electrical properties. The PbTe based thermoelectric generators are used in space crafts, military equipment and pacemakers batteries to name a few [11].

### 1.4 Bi<sub>2</sub>Te<sub>3</sub>

$\text{Bi}_2\text{Te}_3$  (Bismuth telluride) is another conventional and telluride-based thermoelectric material that has been used in the past 50 year. It has a low thermal conductivity of  $1,5 \text{ W}/(\text{m} \cdot \text{K})$  and Seebeck coefficient of  $220 \mu\text{V}/\text{K}$  at room temperature. Highest  $ZT$  value measured for  $\text{Bi}_2\text{Te}_3$  is just over 1,5. The difference with other materials for  $\text{Bi}_2\text{Te}_3$  is the low melting temperature of 858 K and thus a low operating temperature of up to 500 K.

### 1.5 SiGe

SiGe (Silicon-Germanium) alloys have been used for high temperature applications of up to 1170 K, such as radioisotope thermoelectric generators on space crafts [12]. At this temperature the  $ZT$  value of 1,3 has been reached [5]. Although the  $ZT$  values of SiGe at room temperature are lower than  $\text{Bi}_2\text{Te}_3$ , SiGe alloys are much more abundant than Tellurium. Thus, the widespread use of SiGe alloys in thermoelectric generators is more sustainable [12].

### 1.6 Cu<sub>2</sub>Se

$\text{Cu}_2\text{Se}$  (Copper selenide) has been under observation for thermoelectric use since 2010s. The high  $ZT$  values have been reached due to the low thermal conductivity of under  $1 \text{ W}/(\text{m} \cdot \text{K})$ . The Seebeck coefficient of  $\text{Cu}_2\text{Se}$  is around  $300 \mu\text{V}/\text{K}$  at the temperature of

1000 K [9]. With nanostructure engineering resulting in phase transition,  $Cu_2Se$  had significantly better  $ZT$  values of over 1,8 and even over 2,0 at temperature of 850 K [13]. Further  $ZT$  enhancement techniques are being researched.

## 1.7 Skutterudites

Skutterudites have gotten their name from a city in Norway called Skotterud and was discovered by Wilhelm Karl von Haidinger in 1845 [14]. The most studied skutterudites are the ones based on antimony (Sb), mostly because of its low electrical resistivity and good Seebeck coefficient. More specifically the most promising single crystal skutterudite mineral is  $CoSb_3$  (Cobalt antimonide), having a high Seebeck coefficient of  $200 \mu V/K$  but also high thermal conductivity of  $8,9 \text{ W}/(\text{m} \cdot \text{K})$  at 300 K. The highest  $ZT$  values have been achieved by doping the materials with guest atoms, lowering the thermal conductivity and reach over 1,8 at temperature in range of 800 K. For doping such atoms have been used like Yb (Ytterbium), Ba (Barium), In (Indium), Li (Lithium) and Sr (Strontium). With doping, the thermal conductivity has been reduced to lower than  $1 \text{ W}/(\text{m} \cdot \text{K})$  [15].

## 1.8 Other thermoelectric materials

Other thermoelectric materials include half-Heusler alloys,  $Cu_2S$  (Copper(I) sulphide),  $PbS$  (Lead(II) sulphide),  $PbSe$  (Lead selenide),  $SnS$  (Tin(II) sulphide) and  $BiCuSeO$  as seen on figures (Figure 1.1, Figure 1.2). Some of these materials have been synthesized by SPS and many materials have been altered with doping agents or nanostructure engineering (Figure 1.1). Different techniques to improve the  $ZT$  values are being applied along with new materials examined in order to better thermoelectric devices for commercial use.

## 2.REVIEW OF THERMOELECTRIC GENERATORS

### 2.1 Thermoelectric generator working principles

In principal thermoelectric generators (TEGs) consist of two thermoelectric materials: p-type and n-type. P-type and n-type materials have different charge carriers called electrons and electron holes or just holes, respectively. As heat is presented to the thermoelectric materials, holes in p-type material and electrons in n-type material diffuse from hot side to cold side. This in turn creates a potential difference between the cold sides of p-type and n-type materials, and results in a current flow from cold side of p-type material to cold side of n-type material provided they are connected through an electrical circuit. Illustrative figure with heat as input and light from lightbulb as output is shown below (Figure 2.1) [9].

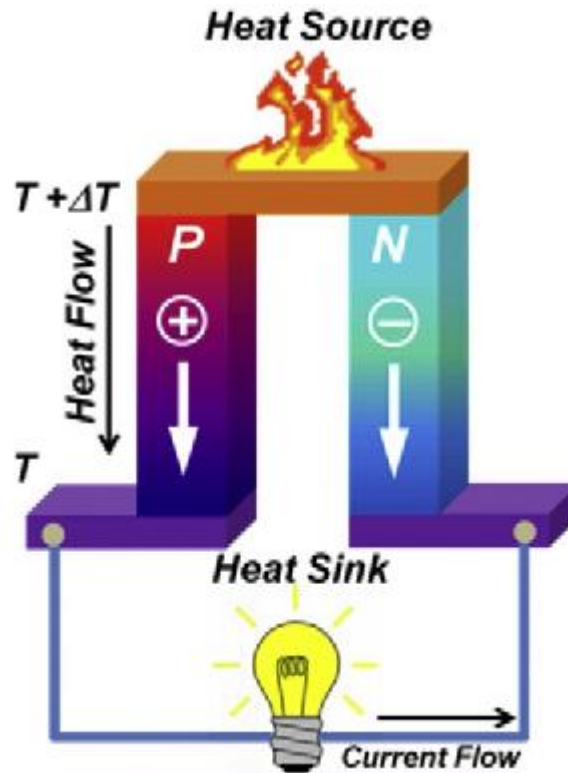


Figure 2.1 Schematic illustration of thermoelectric generator [9]

The overall power generation efficiency of a TEG can be calculated using the average ZT values of both thermoelectric materials and the temperatures from cold and hot side (2.1) [9].

$$\eta_p = \frac{T_h - T_c}{T_h} \left[ \frac{\sqrt{1 + ZT_{ave}} - 1}{\sqrt{1 + ZT_{ave}} + T_c/T_h} \right], \quad (2.1)$$



where  $\eta_p$  – power generation efficiency,

$T_h$  – temperature at hot end, K,

$T_c$  – temperature at cold end, K,

$ZT_{ave}$  – average value of both p-type and n-type legs, wherein  $ZT_{ave}$  per leg is averaged over the temperature dependent  $ZT$  curve between  $T_h$  and  $T_c$  [9].

## **2.2 Thermoelectric generators applications**

The main fields where TEGs are used can be divided to five categories: extreme environments, waste heat recovery, decentralized domestic power and combined heat and power (CHP), micro-generation for sensors and microelectronics and solar TEGs [6]. Thermoelectric generators can be used by direct contact between heat source and TEG or by heat exchanger which transfers the heat via separate water circulation from heat source to TEG.

### **2.2.1 Electricity generation in extreme environments**

Extreme environments usually require a highly reliable energy source over a long period of time. Usually the harsh environment includes very high or very low temperatures, very humid or very dry conditions. Thus, the maintenance frequency must also be very low or non-existent. These types of TEGs are used in space explorations. On spacecrafts the heat is usually produced by the natural decay of radioactive materials. The first TEGs used in space explorations were PbTe based and from 1977 SiGe based TEGs have been used also. Another example of extreme environment where this type of TEGs are used is for industrial applications in remote areas. The Russians have used these TEGs to power lighthouses and navigation beacons. Today TEGs for remote areas are used on gas pipelines, wellheads, offshore platforms, telecommunication sites and for security surveillance and monitoring [6].

### **2.2.2 Waste heat recovery applications**

The main focus on using TEGs in waste heat recovery systems is to reduce the greenhouse gases by using fewer fossil fuels. The most active sector in using TEGs to reduce fuel consumption is transportation including automotive, aeronautics and maritime. The installation of TEG onto vehicle such as cars and trucks is limited by several factors: the pressure loss of exhaust gas cannot be significant, the engine location must stay the same, additional sensors and control units are needed, must be viable in economic perspective. In aeronautics a significant amount of heat is released from the jet engines on planes and turbine engines on helicopters. The most challenging aspect is keeping the TEG cold side cooled without compromising on the weight of the

system. Several studies have been conducted but to date the power density requirements are not met mostly due to added weight of the system to aircrafts. In maritime sector the attractive component for using TEGs is the large and powerful engines used. The heat from the engines at the moment is used to generate fresh water, heat heavy fuel oil and accommodation areas. This decreases the heat to be used in TEGs [6]. Therefore, the heat of exhaust gases could be a promising source for TEGs.

In addition to transportation, industry is also a field where heat is a by-product of the processes. Part of this heat is used for heating networks and in some places converted into electricity by using steam turbines. Steelmaking industry is a sector where a lot of heat is radiant heat from steel products coming from furnace. Several researches have been made to use that radiant heat for TEGs. Same proposal has been made for cement manufacturing plants [6].

### **2.2.3 Decentralized domestic power and CHP generation systems**

In developing countries, an estimated 1,2 billion people do not have access to the electricity grid. Biomass combustion is the main energy source for this population with still having the electrical needs as well. With the very low efficiencies and high toxic emissions from the stoves, deforestation and health risks are the main problems in these areas. If better combustion systems are to be installed, electricity is also necessary to run these systems. In these areas TEGs could be used for charging phones and lighting. Some researches have been made with the focus of installing TEGs to cookers or stoves. Other studies have been made with the focus on increasing the efficiencies of combustion systems by adding fans or smoke extractors using TEGs in those systems. Other wood-stoves with high performance are increasing in quantity in other domestic areas in developed countries also and their control systems need electricity which could be generated with thermoelectric modules [6].

### **2.2.4 Micro-generation for sensors and microelectronics**

Many sensors which are used in products or factories are in remote places or isolated from electricity grids but need very low energy to operate. Powering these devices with wires is therefore expensive or impossible and, in such cases, batteries are used instead. This in turn limits the lifespan of sensors to battery lifespan if no access to change the battery is present. A few square millimetres in size, small TEGs can be a solution to these challenges with good performance in harsh environments and low maintenance [6].

### **2.2.5 Solar thermoelectric generators**

The heat source for TEG in these systems come from the sun. Since the solar intensity on earth is relatively low, amplification of solar intensity is necessary. Concentrating solar intensity with optical systems is an option. Other application suggests using TEGs with solar panels with the placement of TEG being under the solar panel on the cold side. The cold side of solar panel in this application acts as a hot side for TEG [6].

## **3. EXHAUST GAS CLEANING SYSTEMS IN MARITIME**

From different exhaust gas cleaning systems, three are currently in use on-board ships. They include wet scrubbing with absorption, dry scrubbing with absorption and selective catalytic reduction [4]. The mentioned methods target to remove or reduce the concentration of the following gaseous pollutants from marine diesel engine exhausts:  $\text{SO}_2$ ,  $\text{SO}_3$ ,  $\text{CO}$ ,  $\text{NO}$ ,  $\text{NO}_2$ . In addition to gaseous pollutants exhaust gases consist also of particulate matter [4].

### **3.1 Wet scrubbers**

Wet scrubbers are air pollution control devices and operate by scrubbing an exhaust gas with a liquid. In most cases the scrubbing liquid is water and in marine applications seawater [16]. Wet marine scrubbers are designed to remove particulate matter and in addition can remove  $\text{SO}_x$  (sulphur oxides). The absorbed gases from wet scrubbing are converted into benign compounds. Wet scrubbers have been used in marine applications for about 50 years [4].

#### **3.1.1 Wet scrubber working principle**

The principle of wet scrubbing can be divided to three stages: formation of water droplets in a size range of around  $100\ \mu\text{m}$  to  $1000\ \mu\text{m}$ , a method of forcing a contact between water droplets and exhaust gas, removal of water droplets and drying of the cooled and cleaned exhaust gas [4]. As the water droplets have a  $\text{pH}$  of around 8,0 sulphur oxides ( $\text{SO}_2$ ,  $\text{SO}_3$ ) dissolve into water. The high  $\text{pH}$  level of water droplets can be obtained by using seawater, or freshwater with an alkali consumable additive (usually caustic soda). Nitrogen oxides ( $\text{NO}$ ,  $\text{NO}_2$ ) and carbon oxide ( $\text{CO}$ ) have limited solubility to alkaline water and thus pass through the wet scrubbing section. As mentioned, the particulate matter with the size range of  $0,1\ \mu\text{m}$  to  $100\ \mu\text{m}$  in wet scrubbers is also absorbed and therefore removed from the exhaust gas. The absorption of particulate matter divides into three different trapping processes shown in figure (Figure 3.1) [4].

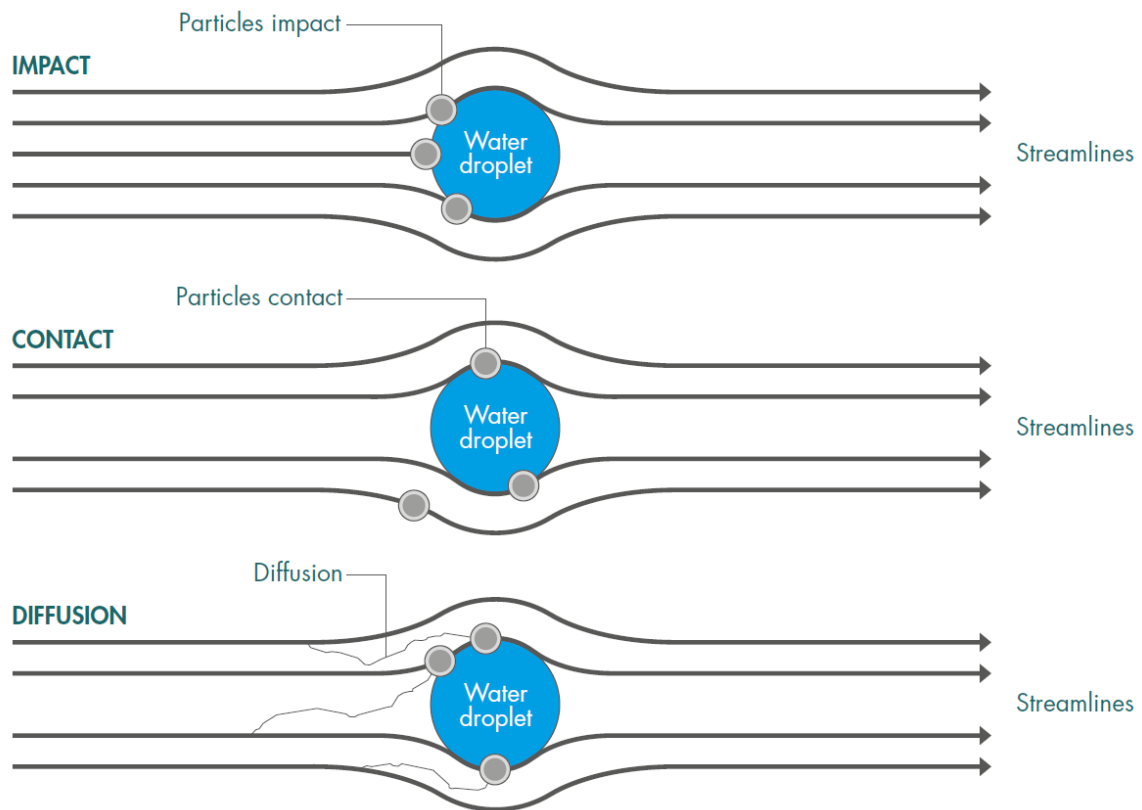


Figure 3.1 Particle trapping processes [4].

The contact and diffusion of particulate matter onto water droplets is more applicable to smaller sizes of matter as larger particles tend not to change their direction of movement. Very small sized particles of less than  $1\ \mu\text{m}$  are absorbed into water droplets mostly by diffusion through random molecular (Brownian) motion. The range of water droplet size is directly related to efficiency of trapping particles. Too small water droplets of less than  $100\ \mu\text{m}$  tend to be carried out of the scrubber with the exhaust gas and too large droplets of more than  $1000\ \mu\text{m}$  have less concentration in scrubbers and reduce the impact probability. Different designs of scrubbers are used for the most effective contact between water droplets and exhaust gas and are shown in the figure (Figure 3.2) [4].

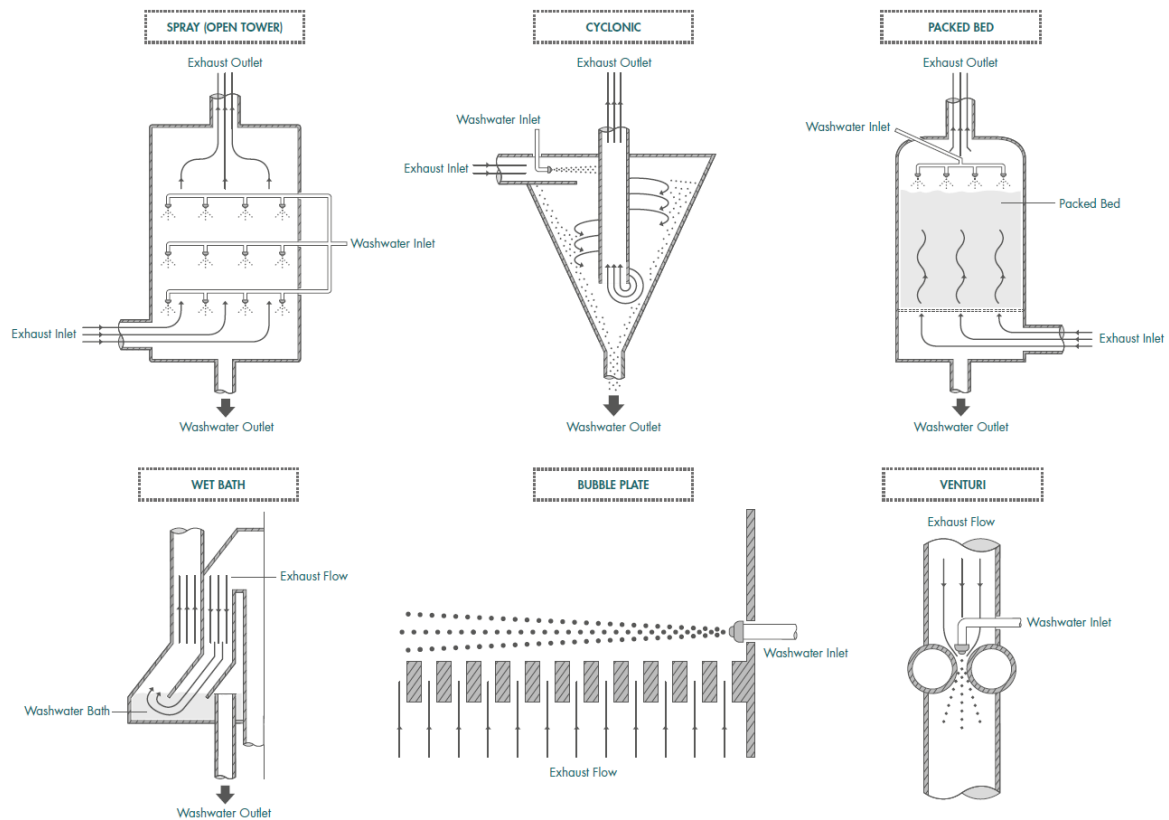


Figure 3.2 Types of wet scrubbers [4].

### 3.1.2 Workflow of wet scrubbers

The first stage when hot exhaust gas enters the scrubber is quenching. The temperature of hot exhaust gas is typically reduced to 333 K with introduction of 10-20 % of whole scrubbing water used. The exhaust gas is cooled adiabatically by expansion and heat transfer to scrubbing water. Thus, the exhaust gas temperature decreases but the overall heat content remains the same. Adiabatically cooled exhaust gas is crucial in order to prevent inefficient scrubbing and formation of salt aerosols in case seawater is used. Furthermore, if exhaust gas flow is low (no expansion) and the temperature remains hot then some water droplets may evaporate prior to collecting pollutants and other droplets may evaporate after collecting pollutants resulting in very low efficiency. In this stage some of the sulphur oxides and particulate matter is removed. The next stage consists a minimum of one stage of scrubbing in which the remaining sulphur oxides are absorbed and particles are trapped. After the main scrubbing stage or stages the water with particulate matter and sulphur oxides saturates on the inner walls of scrubber and is collected at the bottom of the scrubber. After scrubbing the cleaned exhaust gas passes through the demister which is used to collect the remaining water droplets. The demister is also wetted with the remaining water to act as a polishing stage to absorb the remaining of sulphur oxides. Effective designs of scrubbers usually

achieve the removal of sulphur oxides efficiency of 95 to 98 % before exhaust gas enters the demister. The overall efficiency of a wet scrubber depends on the diffusion efficiency of particulate matter, saturation of water that absorbed the sulphur oxides and water temperature [4].

### **3.2 Dry scrubbers**

Dry scrubbers divide into two, based on the absorption methods: physical and chemical absorption. Physical absorption is based on exhaust gas sticking onto the absorbent due to van der Waal's force, but the process is reversible with the increase in heat or gas concentration in surrounding environment.

In marine applications a chemical absorption is used with the absorbent being CaOH (calcium hydroxide or hydrated lime). The efficiency of a dry scrubber depends on the specific surface area of CaOH granules which have the size range from 2 to 8 mm. With the high specific surface area and 50 % of that surface reacting with the exhaust gas a sulphur oxides reduction efficiency of 99 % can be achieved. During this process the temperature of exhaust gas remains the same and therefore the volume as well. In order to remove the particulate matter from the exhaust gas with filter trapping the gas flow rate must be lowered by sufficient sizing of the scrubber. For the removal of smaller particulate matter further development of dry scrubbers is necessary. Therefore the dry scrubbers are not yet very widely used [4].

### **3.3 Selective catalytic reduction (SCR)**

Previously described methods of cleaning the exhaust gas do not target the removal of nitrogen oxides (NO<sub>x</sub>) or have limited capacity to do so. For more effective removal of NO<sub>x</sub> one option is to use SCR along with a scrubber. SCR converts NO<sub>x</sub> into more safer N<sub>2</sub> (nitrogen) and H<sub>2</sub>O (water) by means of a reducing agent absorbed onto a catalyst. Typically, NH<sub>3</sub> (ammonia) is used as reducing agent, formed by the decomposition of CO(NH<sub>2</sub>)<sub>2</sub> (urea) injected into the exhaust gas stream. Injected urea mixed with exhaust gas, specifically water in exhaust gas, forms ammonia. Urea must be mixed with the exhaust gas stream thoroughly in specially designed duct for producing ammonia. Directly using ammonia usually cannot be done due to its hazardous properties with handling it, including toxicity, corrosiveness, and harmfulness to the environment. After the formation of ammonia in the exhaust duct the NO<sub>x</sub> components, NO (nitric oxide) and NO<sub>2</sub> (nitrogen dioxide) coming into contact with the catalyst surface react with ammonia and O<sub>2</sub> (oxygen) from the exhaust. This reaction results with nitrogen and water [4]. The by-product of the reaction is CO<sub>2</sub> (carbon dioxide) but the quantity of

that can be neglected by comparing it with the CO<sub>2</sub> produced by the fuel oil combustion. The layout of SCR is shown in figure (Figure 3.3).

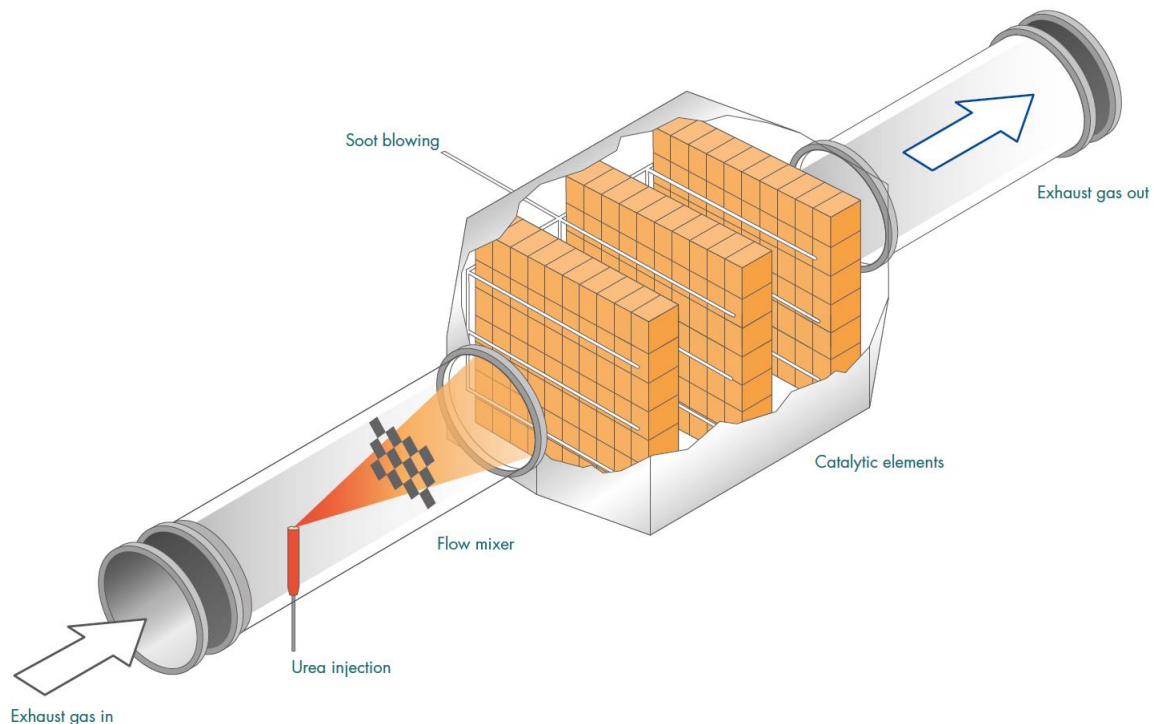


Figure 3.3 Selective Catalytic Reduction unit [4].

The efficiency of SCR is reduced with lower exhaust gas temperatures and engines working at partial load. Typically, SCR systems find its application on four-stroke medium and high speed engines. At normal operating the exhaust gas temperature should be over 570 K. NO<sub>x</sub> emissions can be reduced by up to 90 % with SCR [4].

### 3.4 Exhaust gas recirculation (EGR)

During the operation of engine a reaction in charge air takes place between nitrogen and oxygen resulting in formation of nitric oxide. Most of the nitric oxide is formed thermally and depends on the temperature in the combustion zone. Significant formation of nitric oxide takes place at temperatures of 1470 K and rise exponentially with temperatures over 1770 K. Secondary factors contributing to NO<sub>x</sub> formation are the amount of oxygen available due to excess air within the combustion zone and the time of combustion gas exposed to high temperatures. Leaving the combustion chamber some of the NO is oxidised to form NO<sub>2</sub>. Most improvement in reducing the formation of NO<sub>x</sub> has been found in optimizing and adjusting the operation of engines. The parameters of engine operation to reduce NO<sub>x</sub> formation include pressure, timing and rate of fuel injection, fuel nozzle configuration, exhaust valve timing, the temperature and pressure of excess air, and compression ratio. Adjusting these parameters lower



the combustion zone temperatures and oxygen levels. This technology has been used in on-road applications and has been applied to large two-stroke marine diesel engines. With the mixture of fresh air and recirculated air from exhaust gas the peak combustion temperature is lowered and thus the formation of NO. The EGR system is typically used with wet scrubbers to clean the recirculated exhaust gas from SO<sub>x</sub> and particulate matter. In practice more than 50 % of NO<sub>x</sub> reduction has been achieved and up to 85% reduction is proposed [4].

## 4. CASE DESCRIPTION

The case researched in this paper is for the Clean Marine's EGCS (Exhaust gas cleaning system) 100k wet scrubber and the integration possibility of TEG unit to that. The number in the name indicates the exhaust gas mass flow of 100 000 kg/h for which the scrubber was designed. In operation the mass flow rate of exhaust gas is smaller [17]. Figure 4.1 shows the overall movement of exhaust gas to and from the EGCS.

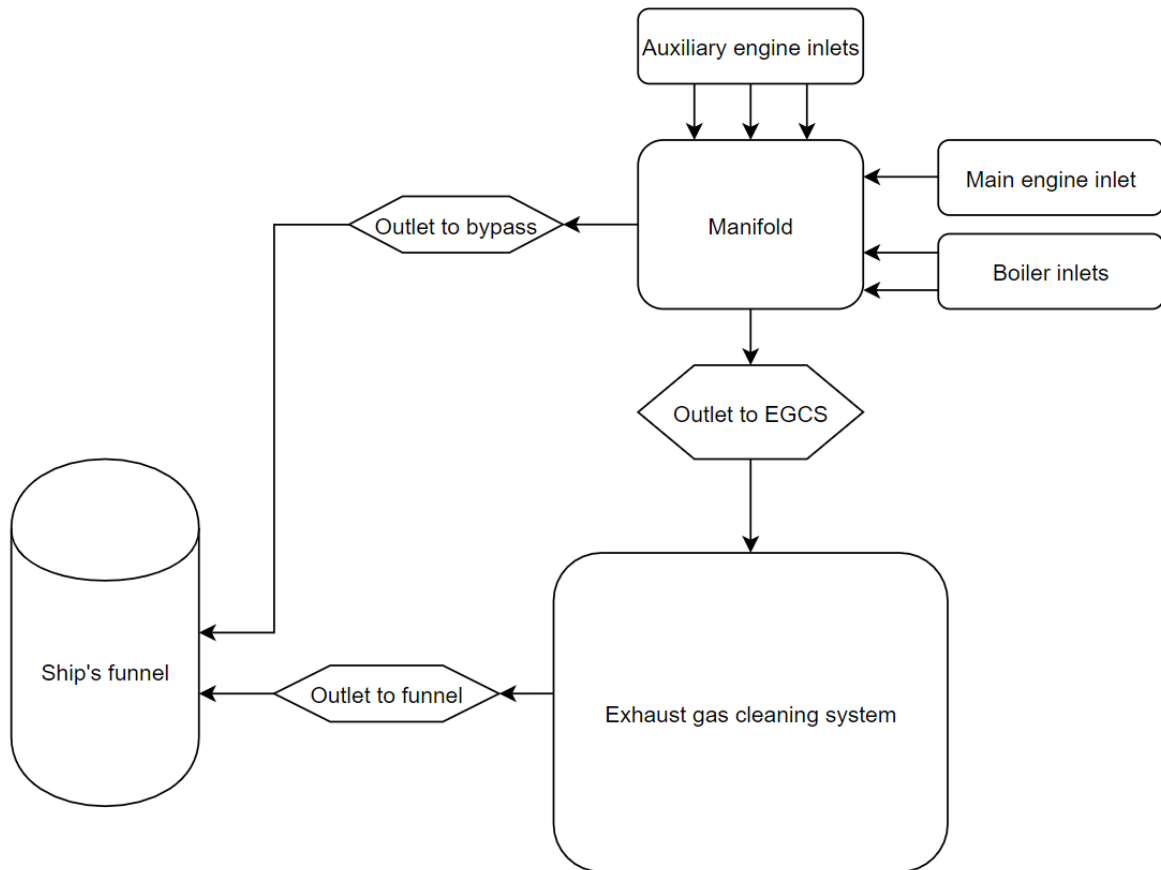


Figure 4.1 Overall exhaust gas movement to and from the EGCS [17]

All exhaust gases from main engine, auxiliary engines and boilers go through the manifold. From there is an option to bypass the scrubber in case maintenance needs to be done during vessel operation. 90% of the time in a year the scrubber is operating, and exhaust gas is not bypassing the EGCS [17]. From the scrubber the exhaust gas leaves the vessel through the ship's funnel. The Figure 4.2 shows the exhaust gas and seawater movement through the scrubber itself.

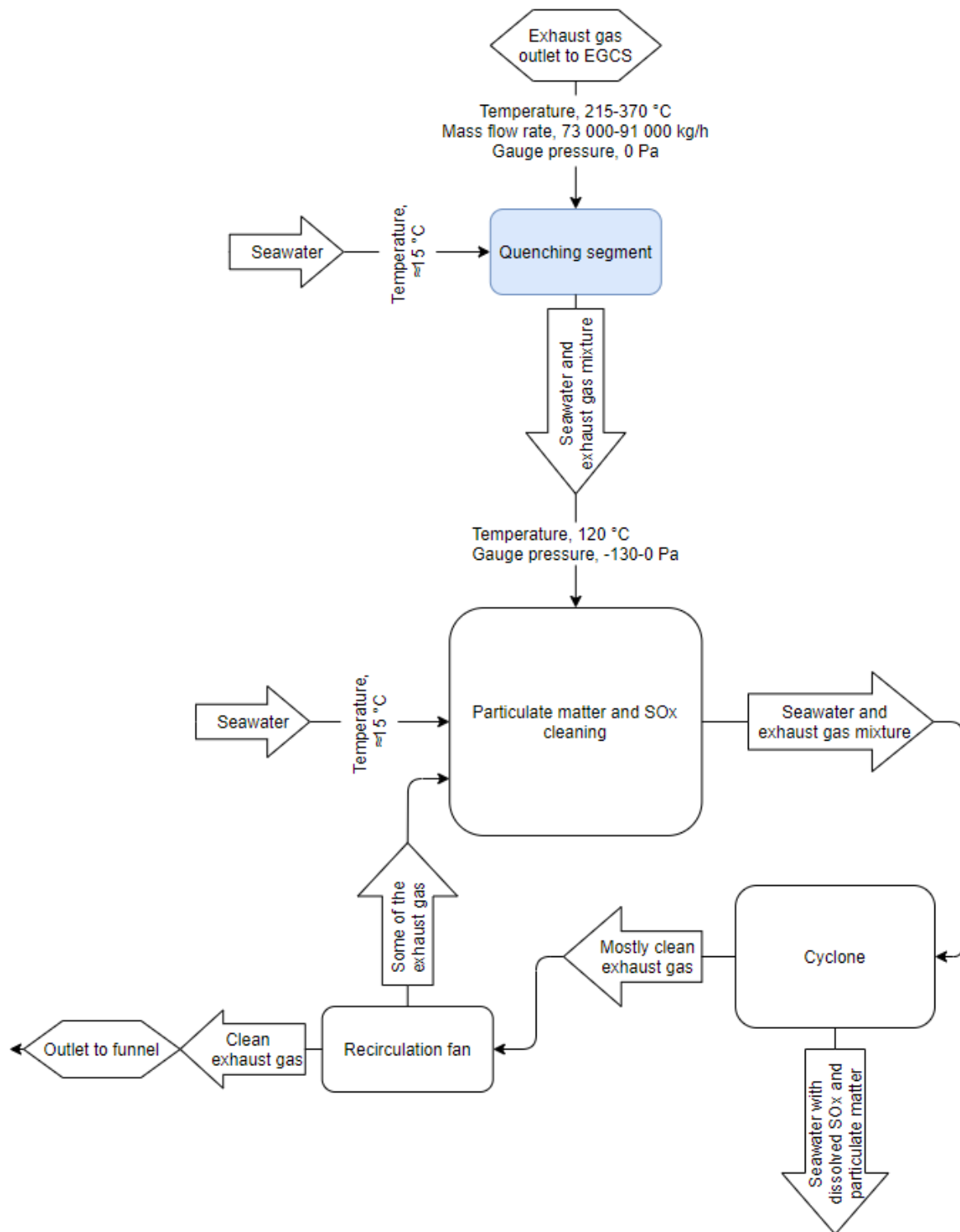


Figure 4.2 Exhaust gas movement through the EGCS [17]

As described before, for wet scrubbers the first section is the quenching segment in which the temperature of the exhaust gas is significantly lowered by spraying water to the exhaust gas stream. As mentioned above the quenching (rapid cooling of exhaust gas) is required to minimise the water evaporation possibility in the scrubbing zone. The aim is to replace that segment with TEG system and neglect the usage of seawater in

the first section. Figure 4.3 shows the flow chart of TEG system integration to wet scrubber. The physical space of quenching segment would be replaced by the heat exchanger. Other sections of the wet scrubber would remain the same. Leaving the quenching segment, more seawater is added to the exhaust gas stream and particulate matter and  $\text{SO}_x$  is scrubbed. From that section seawater and exhaust gas mixture enters the cyclone where seawater containing  $\text{SO}_x$  and particulate matter is separated from rest of the exhaust gas. The exhaust gas then enters the recirculation fan and depending on the extent of cleaning efficiency it is recirculated back to the main scrubbing zone or leaves the vessel through the ship's funnel.

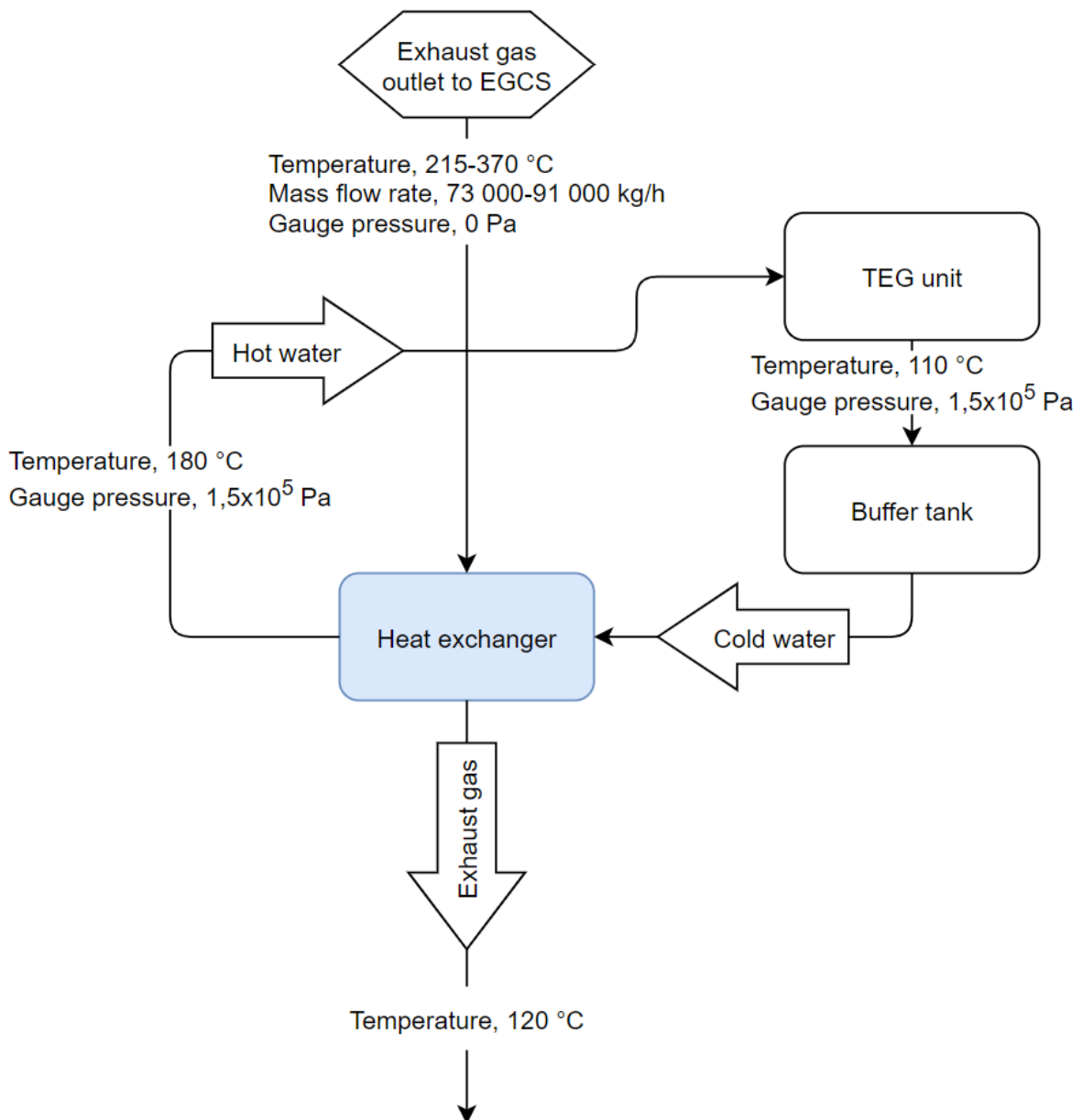


Figure 4.3 Exhaust gas movement through EGCS with integrated TEG unit [17]

Ideally the heat exchanger of the TEG system would lower the exhaust gas temperature fast enough to replace the quenching segment entirely. From the heat exchanger,

heated water would be used as the input power for the TEG unit. In case the heat exchanger could not lower the temperature of exhaust gas fast enough, the quenching segment can be replaced partially and the end result would be a combination of flow charts from Figure 4.2 and Figure 4.3. In that case, half of the temperature would be lowered by heat exchanger and half by spraying seawater to the gas stream. The replacement has spatial constraints set by the height of current quenching segment. Thus, relatively the same sized heat exchanger is considered which then would have to be efficient and compact. The key parameters and characteristics of exhaust gas, quenching segment (Table 4.1), exhaust gas composition (Table 4.2), water parameters, connecting the heat exchanger and TEG unit (Table 4.3), and heat exchanger itself (Table 4.4) are shown below. The parameters of exhaust gas shown in Table 4.1 is for initial calculation based on information from Clean Marine and can be further adjusted in the range shown in Figure 4.2.

Table 4.1 Exhaust gas and quenching segment parameters obtained from Clean Marine AS [17], [18]

| <b>Parameter</b>   | <b>Unit</b>       | <b>Value</b>         |
|--|-------------------|----------------------|
| Mass flow rate, $M_1$                                    | kg/h              | 73 000               |
| Gauge pressure in scrubber, $P_1$                        | Pa                | 0                    |
| Temperature entering quenching, $T'_1$                   | K                 | 565,65               |
| Temperature exiting quenching, $T''_1$                   | K                 | 393,15               |
| Arithmetic average temperature, $\Delta t_{m1}$          | K                 | 479,4                |
| Molar mass of exhaust gas, $M_{EG}$                      | kg/kmol           | 28,82                |
| Kinematic viscosity at $\Delta t_{m1}$ , $\nu_{EG}$      | m <sup>2</sup> /s | $3,36 \cdot 10^{-5}$ |
| Thermal conductivity at $\Delta t_{m1}$ , $\lambda_{EG}$ | W/(m · K)         | 0,041                |
| Prandtl number at $\Delta t_{m1}$ , $Pr_{EG}$            |                   | 0,65                 |
| Prandtl number at $T_{tube}$ , $Pr_{EGS}$                |                   | 0,69                 |
| Height of quenching segment, $H_{QS}$                    | m                 | 2,4                  |
| Diameter of quenching segment, $D_{QS}$                  | m                 | 1,9                  |

The arithmetic average temperature for exhaust gas is calculated with the equation (4.1).

$$\Delta t_{m1} = \frac{T'_1 + T''_1}{2} = \frac{565,65 + 393,15}{2} = 479,40 \text{ K}, \quad (4.1)$$

Table 4.2 Composition of exhaust gas [17]

| Element          | Partial mass, kg/kg |
|------------------|---------------------|
| N <sub>2</sub>   | 0,748               |
| CO <sub>2</sub>  | 0,063               |
| H <sub>2</sub> O | 0,027               |
| O <sub>2</sub>   | 0,162               |

Since other elements in exhaust gas have insignificant partial mass, the calculations done based on exhaust gas composition neglect those elements [17].

Table 4.3 Water (connecting heat exchanger and TEG) parameters [17], [19]

| Parameter   | Unit              | Value                 | Source                      |
|---|-------------------|-----------------------|-----------------------------|
| Gauge pressure, $P_w$   | Pa                | $1,5 \times 10^5$     | Clean Marine                |
| Inlet temperature, $T'_2$   | K                 | 383,15                | Clean Marine                |
| Outlet temperature, $T''_2$   | K                 | 453,15                | Clean Marine                |
| Average temperature, $T_{2AVG}$                                     | K                 | 418,15                | Based on $T'_2$ and $T''_2$ |
| Specific enthalpy at $T'_2$ , $h'_2$                                | J/kg              | 461 368               | IAPWS-IF97                  |
| Specific enthalpy at $T''_2$ , $h''_2$                              | J/kg              | 2 833 207             | IAPWS-IF97                  |
| Density at $T_{2AVG}$ and $P_w$ , $\rho_w$                          | kg/m <sup>3</sup> | 0,788                 | IAPWS-IF97                  |
| Thermal conductivity of water at $T_{2AVG}$ and $P_w$ , $\lambda_w$ | W/(m · K)         | 0,0285                | IAPWS-IF97                  |
| Prandtl number of water at $T_{2AVG}$ and $P_w$ , $Pr_w$            |                   | 0,994                 | IAPWS-IF97                  |
| Kinematic viscosity of water at $T_{2AVG}$ and $P_w$ , $\nu_w$      | m <sup>2</sup> /s | $1,77 \times 10^{-5}$ | IAPWS-IF97                  |

Using the equation (4.1) the arithmetic average temperature of,  $T_{2AVG}$ , water was obtained.

Table 4.4 Heat exchanger parameters [17], [20], [21]

| Parameter   | Unit           | Value | Source       |
|---|----------------|-------|--------------|
| Heat exchanger/quenching segment height, $H_{HE}$ | m              | 2,4   | Clean Marine |
| Heat exchanger cross-section area, $A_{HE}$       | m <sup>2</sup> | 1,6   | Clean Marine |

Table 4.4 continued

| Parameter   | Unit      | Value     | Source                                |
|---|-----------|-----------|---------------------------------------|
| Single tube length in heat exchanger, $L_{HE}$            | m         | 1,265     | Based on cross-section area           |
| Width of heat exchanger, $W_{HE}$                         | m         | 1,265     | Based on cross-section area           |
| Tube material   |           | EN 1.4401 | Clean Marine                          |
| Tube outer diameter, $D_o$                                | mm        | 28,0      | Assumption                            |
| Tube outer radius, $r_o$                                  | mm        | 14,0      | Based on $D_o$                        |
| Tube wall thickness, $t_p$                                | mm        | 2,0       | Assumption                            |
| Tube inner diameter, $D_I$                                | mm        | 24,0      | Based on $D_o$ and $t_p$              |
| Tube inner radius, $r_I$                                  | mm        | 12,0      | Based on $t_p$                        |
| Diameter of a rib, $D_r$                                  | mm        | 50,0      | Assumption                            |
| Rib thickness, $t_r$                                      | mm        | 2,0       | Assumption                            |
| Radius of a rib, $r_r$                                    | mm        | 25,0      | Based on $D_r$                        |
| Width of a rib, $W_r$                                     | mm        | 11,0      | Based on $r_r$ and $r_o$              |
| Spacing between ribs, $S_r$                               | mm        | 4,0       | Assumption                            |
| Distance between tubes in a layer, $S_T$                  | mm        | 50,0      | Based on $D_r$                        |
| Aligned distance between tubes in different layers, $S_D$ | mm        | 50,0      | Based on $D_r$                        |
| Distance between layers, $S_L$                            | mm        | 43,3      | Based on $S_T$ and $S_D$              |
| Number of tubes in a layer, $N_{TL}$                      |           | 25        | Based on $S_T$ and $W_{HE}$           |
| Number of layers in heat exchanger, $N_{layer}$           |           | 55        | Based on $S_L$ and $H_{HE}$           |
| Number of tubes in heat exchanger, $N_{tube}$             |           | 1375      | Based on $N_{TL}$ and $N_{layer}$     |
| Average temperature of tube, $T_{tube}$                   | K         | 448,78    | Calculated                            |
| Thermal conductivity of tube at $T_{tube}$ , $\lambda_t$  | W/(m · K) | 16,0      | From thermal conductivity tables [21] |

The arithmetic average temperature of tube,  $T_{tube}$ , was calculated with the equation (4.2).

$$T_{tube} = \frac{T_1' + T_1'' + T_2' + T_2''}{4} = \frac{565,65 + 393,15 + 383,15 + 453,15}{4} = 448,78 \text{ K}, \quad (4.2)$$

where  $T_{tube}$  – average temperature of the tube, K,

$T_1'$  – exhaust gas inlet temperature, K,

$T_1''$  – exhaust gas outlet temperature, K,

$T_2'$  – water inlet temperature, K,

$T_2''$  – water outlet temperature, K.

Dimensions shown in Table 4.4 have the corresponding symbols presented in Figure 4.4 and Figure 4.5.

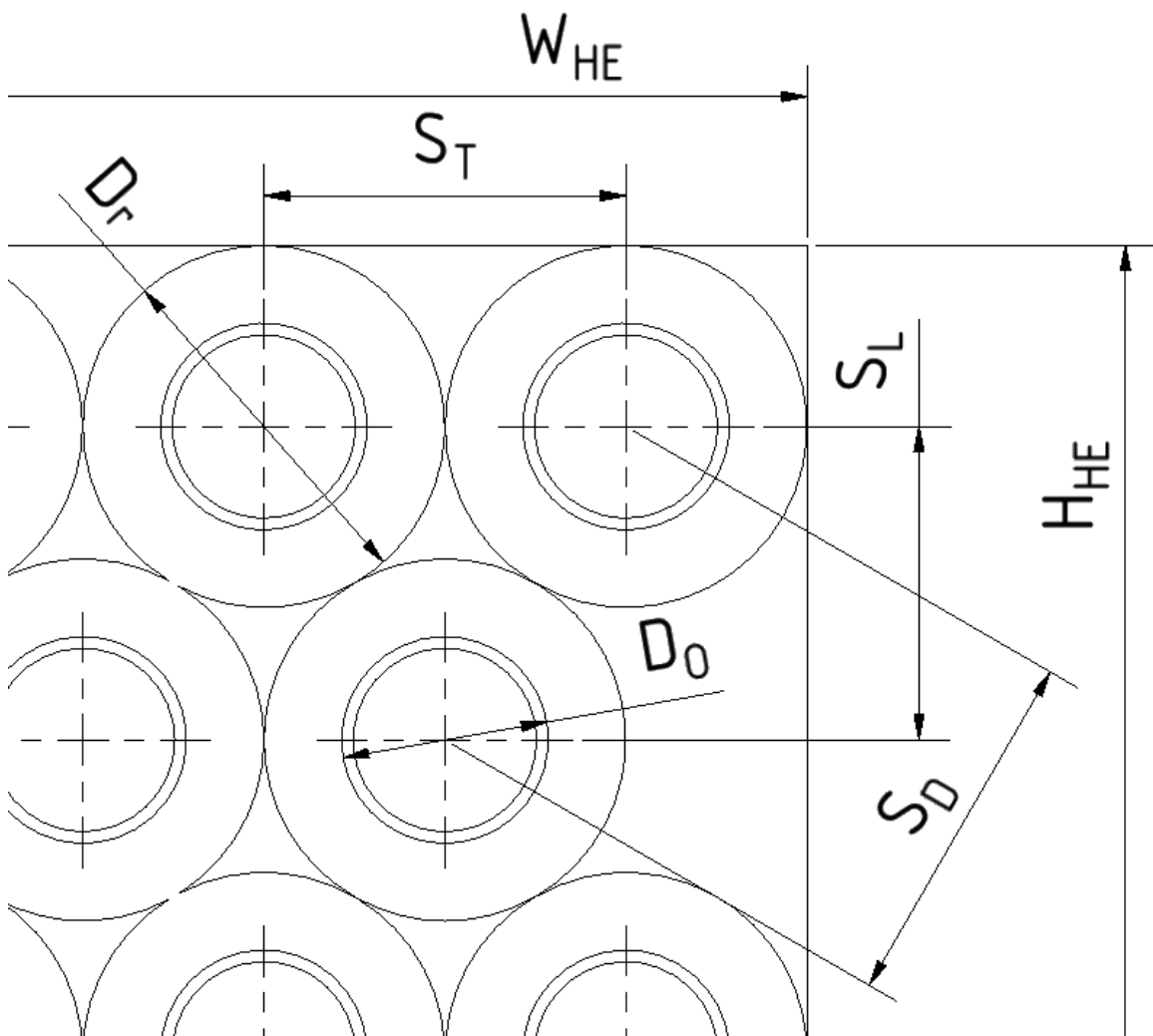


Figure 4.4 Schematic structure of tubes in heat exchanger [17]



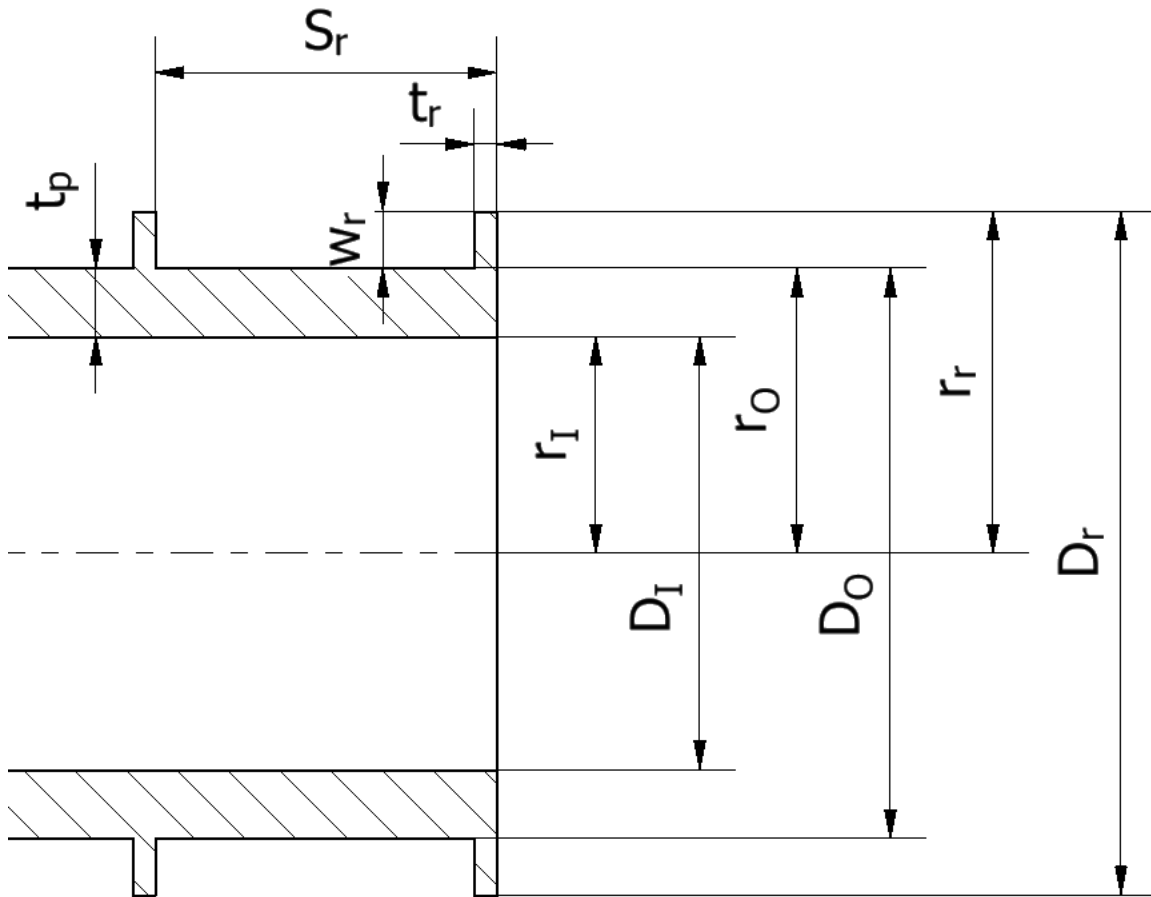


Figure 4.5 Tube and rib dimensions [17]

Since the width in both directions of the heat exchanger is the same, heat exchanger width  $W_{HE}$  and length of straight tube piece  $L_{HE}$  was calculated with the equation (4.3) [17].

$$W_{HE} = L_{HE} = \sqrt{A_{HE}} = \sqrt{1,6} = 1,265 \text{ m.} \quad (4.3)$$

The distance between layers in the heat exchanger,  $S_L$ , can be calculated with the equation

$$S_L = \sqrt{S_D^2 - \left(\frac{S_T}{2}\right)^2} = \sqrt{0,05^2 - \left(\frac{0,05}{2}\right)^2} = 0,0433 \text{ m.} \quad (4.4)$$

Since distance between tubes in a layer,  $S_T$ , and aligned distance between tubes in different layers,  $S_D$ , are the same, all the ribs can have the same diameter and therefore radius and width. Based on the radiuses of rib  $r_r=25$  mm and tube  $r_o=0,014$  mm, the width of a rib was calculated with the equation (4.5).

$$W_r = r_r - r_o = 25 - 14 = 11 \text{ mm} = 0,011 \text{ m.} \quad (4.5)$$

The heat exchanger used in this application based on the given information has a staggered tube bank with ribs on tubes and has a cross-flow between water and exhaust gas [17]. Several assumptions had to be made regarding the dimensions of tubes and ribs of the heat exchanger. After initial calculations on the properties of the heat exchanger, further optimisation is done.

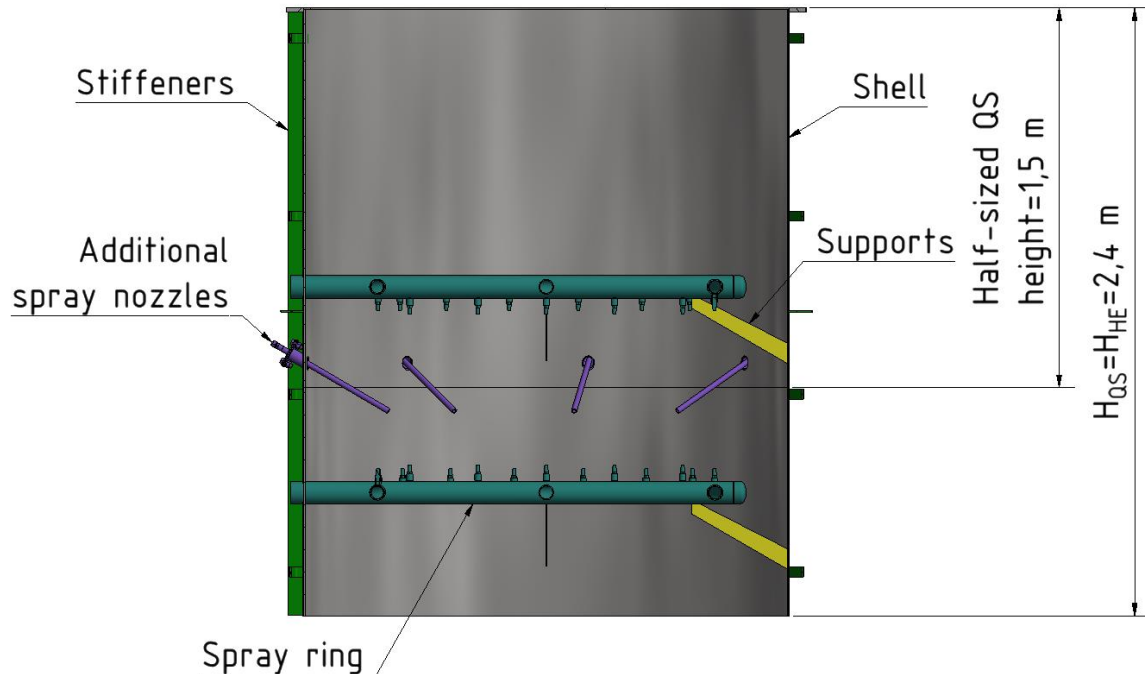


Figure 4.6 Section view of quenching segment [17]

The dimensions and parts of quenching segment are shown in Figure 4.6 and Figure 4.7. The segment consists of 2 spray rings and 8 additional spray nozzles spraying seawater to reduce the exhaust gas temperature. The shell is from material EN 1.4547 or commonly known as SMO254 and the spray sections and additional spray nozzles made from pipes as well as support plates inside are from material EN 1.4410, commonly known as Super Duplex. Stiffeners on the outside are made from material EN 1.4404 [17].

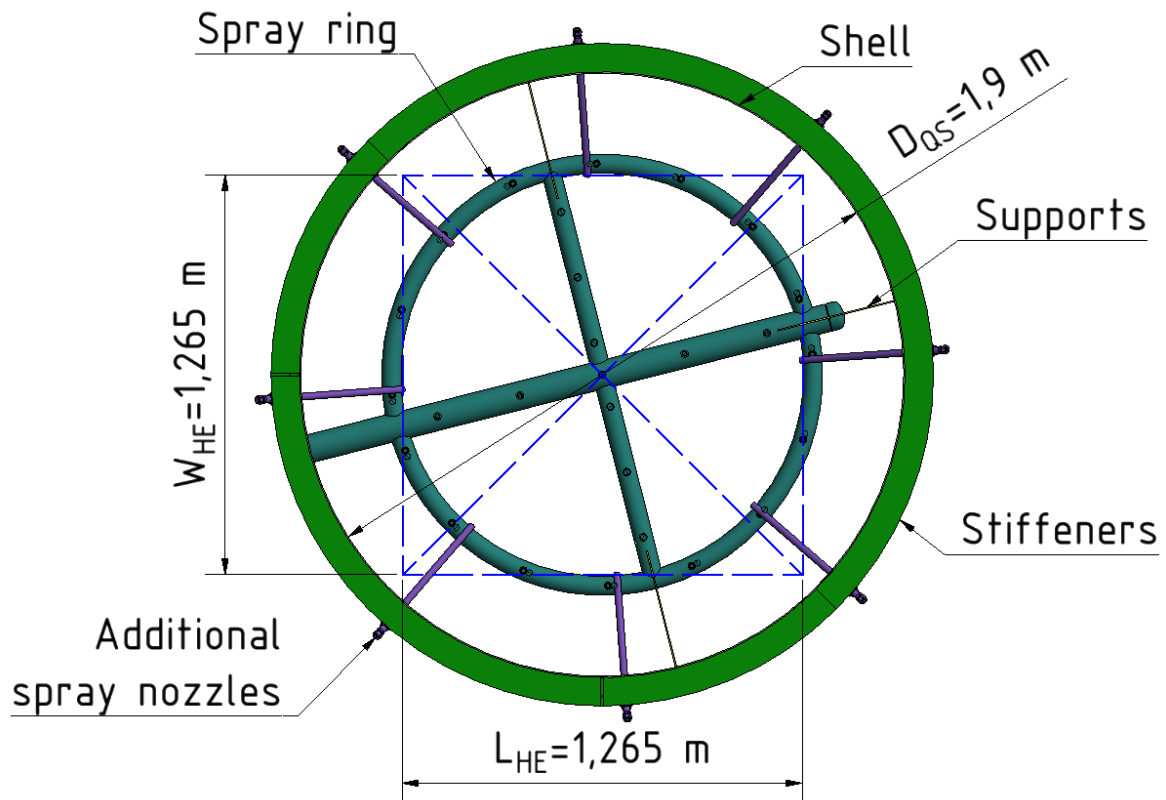


Figure 4.7 Cross-section view of quenching segment [17]

In Table 4.5 and Table 4.6 are shown the prices of the parts for full-sized and half-sized quenching segments, respectively. Detailed part list of all the parts and prices is shown in Appendix 2 below.

Table 4.5 Prices of parts for full-sized quenching segment [17], [22]

| Description              | Main material | Price, €        |
|--------------------------|---------------|-----------------|
| Shell                    | EN 1.4547     | 8052,96         |
| Spray rings              | EN 1.4410     | 2261,51         |
| Additional spray nozzles | EN 1.4410     | 289,62          |
| Stiffeners               | EN 1.4404     | 1679,68         |
| Supports                 | EN 1.4547     | 178,44          |
|                          | <b>Sum</b>    | <b>12462,20</b> |

Table 4.6 Prices of parts for half-sized quenching segment [17], [22]

| Description              | Main material | Price, € |
|--------------------------|---------------|----------|
| Shell                    | EN 1.4547     | 4534,76  |
| Spray rings              | EN 1.4410     | 1130,75  |
| Additional spray nozzles | EN 1.4410     | 144,81   |

Table 4.6 continued

| <b>Description</b> | <b>Main material</b> | <b>Price, €</b> |
|--------------------|----------------------|-----------------|
| Stiffeners         | EN 1.4404            | 1469,85         |
| Supports           | EN 1.4547            | 89,22           |
|                    | <b>Sum,</b>          | <b>7369,39</b>  |

The price of half-sized quenching segment (Table 4.6) is based on using half of the nozzles to spray seawater and all the parts in correlation with those. The cost of manufacturing full-sized and half-sized quenching segment along with material cost are shown in Table 4.7.

Table 4.7 Total costs of material and manufacturing of different sized quenching segments [17]

| <b>Type of cost</b>             | <b>Price (Full-sized), €</b> | <b>Price (Half-sized), €</b> |
|---------------------------------|------------------------------|------------------------------|
| Material                        | 12462,20                     | 7369,39                      |
| Manufacturing                   | 3818,12                      | 2464,54                      |
| <b>Sum, <math>C_{mf}</math></b> | <b>16280,32</b>              | <b>9833,93</b>               |

Methods described in chapter 5 are with the aim to equalize the needed reduction of exhaust gas temperature with the heat exchanger's ability cool the exhaust gas to desired temperature. The possibility of replacing the quenching segment and integrating the TEG unit is ultimately due to the high price of material and manufacturing cost to produce the quenching segment [17]. If the first option of replacing quenching segment entirely is not feasible, calculations are made to replace half of the quenching segment. If desired outcome is not possible for either of the cases, the TEG system would be integrated to the ship's structure separately from wet scrubber.

## 5. METHOD TO EVALUATE THE POSSIBILITY OF REPLACING QUENCHING SEGMENT WITH TEG SYSTEM

Methods described in this paragraph are to evaluate the possibility of replacing the quenching segment of the wet scrubber with TEG system.

Since a pressure drop occurs on either side of the heat exchanger, it can be considered in financial calculations. For other applications the corrosion resistance is an aspect to consider with. In this case the material of the heat exchanger (Table 4.4) and the acid bath surface treatment prevent corrosion to be a considerable factor in these calculations [17].

### 5.1 The rate of heat exchange

Quenching process in scrubbers is essential to lower the exhaust gas temperature as described previously in the paragraph of wet scrubbers (3.1 Wet scrubbers). To lower the temperature, a certain amount of heat needs to be transferred from the exhaust gas to the TEG system. The TEG system in itself contains a heat exchanger which is placed into the stream of exhaust gas. The heat exchange rate must be sufficient to lower the exhaust gas temperature to desired value. The rate of heat exchange can be calculated with the equation (5.1) below [23]. The method is valid with the assumption that the heat exchange to external environment is neglected and can be used if one or the other substance goes through a phase change.

$$Q = M_1(h'_1 - h''_1) = M_2(h''_2 - h'_2), \quad (5.1)$$

where  $Q$  – rate of heat exchange, W,

$M_1$  – mass flow rate of exhaust gas, kg/s,

$h'_1$  – specific enthalpy of exhaust gas at the inlet of heat exchanger, J/kg,

$h''_1$  – specific enthalpy of exhaust gas at the outlet of heat exchanger, J/kg,

$M_2$  – mass flow rate of water, kg/s,

$h''_2$  – specific enthalpy of water at the outlet of heat exchanger, J/kg,

$h'_2$  – specific enthalpy of water at the inlet of heat exchanger, J/kg.

The  $(h'_1 - h''_1)$  and  $(h''_2 - h'_2)$  parts of the equation express the difference in specific enthalpy of exhaust gas and water, and can be shown as  $\Delta h_1$  and  $\Delta h_2$  respectively with equation (5.2).

$$\Delta h = h' - h'', \quad (5.2)$$

where  $\Delta h$  – difference in specific enthalpy, J/kg,

$h'$  - specific enthalpy of substance entering the heat exchanger, J/kg,

$h''$  - specific enthalpy of substance exiting the heat exchanger, J/kg.

The difference in specific enthalpy is therefore the amount of heat transferred for a unit of mass and can be calculated with the equation (5.3) [23].

$$\Delta h = c_{mp} \Big|_{T_2}^{T_1} (T_1 - T_2), \quad (5.3)$$

where  $\Delta h$  - the difference in specific enthalpy, J/kg,

$c_{mp} \Big|_{T_2}^{T_1}$  – the average specific heat between temperature range from  $T_2$  to  $T_1$ , J/(kg · K),

$T_1$  – the temperature of substance entering the heat exchanger, K,

$T_2$  – the temperature of substance exiting the heat exchanger, K.

For both equations, (5.2) and (5.3), values of entering and exiting the heat exchanger must be exchanged for water because water in this case gains heat. Since the derivative of enthalpy by temperature is equal to the isobaric specific heat of a substance, isobaric specific heat must be used for the equation (5.3) [23]. For calculating the average specific heat of exhaust gas, polynomial equations can be used [18]. Equation below (5.4) can be used to calculate the average isobaric specific heat of an exhaust gas for a given temperature range [24].

$$c_{mp} \Big|_{t_2}^{t_1} = \frac{c_{p1}t_1 - c_{p2}t_2}{t_1 - t_2}, \quad (5.4)$$

where  $c_{mp}$  – average isobaric specific heat of exhaust gas for temperature range from  $t_1$  to  $t_2$ , J/(kg · K),

$c_{p1}$  – average isobaric specific heat of exhaust gas for temperature range from 0 °C to  $t_1$ , J/(kg · K),

$c_{p2}$  – average isobaric specific heat of exhaust gas for temperature range from 0 °C to  $t_2$ , J/(kg · K),

$t_1$  – temperature of gas at the inlet of heat exchanger, °C,

$t_2$  – temperature of gas at the outlet of heat exchanger, °C.

Further calculations on how  $c_{p1}$  and  $c_{p2}$  are obtained are given in the Appendix 1 below. The temperatures used in equation (5.4) are in °C and therefore have to be converted from K.

## 5.2 Properties of the heat exchanger

After the desired rate of heat exchange between exhaust gas and water is calculated the properties of the heat exchanger must meet the criteria to provide the desired

cooling of the exhaust gas and TEG with water at given temperatures, flow rate and pressure. The properties of heat exchanger are expressed with the following equation (5.5) [21], [23].

$$Q_{HE} = k_m F \Delta t_m = \frac{\Delta t_m}{R}, \quad (5.5)$$

where  $Q_{HE}$  – rate of heat exchange of the heat exchanger, W,

$k_m$  – average heat transfer coefficient,  $W/(m^2 \cdot K)$ ,

$F$  – surface area of the heat exchanger,  $m^2$ ,

$\Delta t_m$  – average temperature difference of exhaust gas and water, K,

$R$  – overall thermal resistance,  $W/K$ .

The average temperature difference between exhaust gas and water depends on the direction of flow of exhaust gas and water. For parallel flow, the logarithmic average temperature difference is used and can be calculated with the following equation (5.6).

The same equation can be used for cross-flow and counter-flow [23].

$$\Delta t_m = \frac{\Delta t_l - \Delta t_s}{\ln \frac{\Delta t_l}{\Delta t_s}}, \quad (5.6)$$

where  $\Delta t_m$  – average temperature difference of exhaust gas and water, K,

$\Delta t_l$  – largest temperature difference between exhaust gas and water, K,

$\Delta t_s$  – smallest temperature difference between exhaust gas and water, K.

Some of these parameters might be given including the temperatures of exhaust gas at the inlet and the desired temperature at the outlet of heat exchanger. This also gives the constraints for the inlet and outlet temperatures of water in the heat exchanger. The water temperature at the inlet of heat exchanger cannot be higher than desired exhaust gas temperature at the outlet and the water temperature cannot be higher at the outlet of the heat exchanger than the exhaust gas temperature at the inlet.

### 5.3 Overall thermal resistance

The overall thermal resistance (OTR) is a key figure in meeting the needed outlet temperature of exhaust gas. Since the overall thermal resistance is for all surfaces in the heat exchanger and the average heat transfer coefficient could be derived from that based on the selected surface and the corresponding thermal resistance, the OTR is calculated. Exchanging heat between exhaust gas and liquid leaves the side of the gas always with a higher thermal resistance and therefore it is more determining figure in OTR. For this reason, most heat exchangers with these substances have a ribbed surface

on the side of the gas and surface efficiency must be considered. The overall thermal resistance can be calculated with the following equation (5.7) [21].

$$R = \frac{1}{\eta_0 k_h A_t} + R_w + \frac{1}{k_c A_c}, \quad (5.7)$$

where  $R$  – overall thermal resistance, W/K,

$\eta_0$  – overall surface efficiency on the hot side of heat exchanger,

$k_h$  – heat transfer coefficient between exhaust gas and heat exchanger, W/(m<sup>2</sup> · K),

$A_t$  – total outer surface area of heat exchanger, m<sup>2</sup>,

$R_w$  – thermal resistance of heat exchanging tube, W/K,

$k_c$  – heat transfer coefficient between water and heat exchanger, W/(m<sup>2</sup> · K),

$A_c$  – overall inner surface area of heat exchanger, m<sup>2</sup>.

Sometimes the fouling factor on the hot and cold side are taken into account also, but for this case it is neglected based on the information that regular cleaning of the tubes is done and no significant decrease in efficiency has been noted thus far [17]. The key factor for calculating values in equation (5.7) is the direction of cross-flow between exhaust gas and water [17].

The overall surface efficiency on the exhaust gas side can be calculated with the following equation (5.8) [21].

$$\eta_0 = 1 - \frac{N_r A_r}{A_t} (1 - \eta_r), \quad (5.8)$$

where  $\eta_0$  – overall surface efficiency on the hot side of heat exchanger,

$N_r$  – the total number of ribs in the heat exchanger,

$A_r$  – surface area of a single rib, m<sup>2</sup>,

$A_t$  – total outer surface area of heat exchanger, m<sup>2</sup>,

$\eta_r$  – surface efficiency of a single rib.

The heat exchanger has a staggered tube bank through which the exhaust gas flows. Taking part in the heat exchanging are straight tubes which are connected by elbows outside the active heat exchanging volume. The number of ribs on the surface of tube can be calculated with equation (5.9).

$$N_r = \frac{L_{HE}}{S_r} N_{tube}, \quad (5.9)$$

where  $N_r$  – the total number of ribs in the heat exchanger,

$L_{HE}$  – Length of one tube in heat exchanger, m,

$N_{tube}$  – number of tubes in a heat exchanger,

$S_r$  – spacing between ribs, m.



The number of straight tubes in a heat exchanger can be determined by the width and height of the heat exchanger divided by the spacing between tubes in one layer and spacing between layers in the heat exchanger, respectively. The total number of straight tubes in a heat exchanger is calculated based on the tube and rib sizes. The efficiency and surface area of the rib depends on the shape of the rib itself. The rib shape given for the heat exchanger is rectangular, thus the efficiency of a single  $\eta_r$  rib is expressed with the following equation (5.10) [21].

$$\eta_r = \frac{\tanh \left[ \sqrt{\frac{2k_h}{\lambda_t t_r w_r}} \left( w_r + \frac{t_r}{2} \right)^{3/2} \right]}{\sqrt{\frac{2k_h}{\lambda_t t_r w_r}} \left( w_r + \frac{t_r}{2} \right)^{3/2}} \quad (5.10)$$

where  $\eta_r$  – surface efficiency of a single rib,

$k_h$  – heat transfer coefficient between exhaust gas and heat exchanger,  $W/(m^2 \cdot K)$ ,

$\lambda_t$  – thermal conductivity of a tube in heat exchanger,  $W/(m \cdot K)$ ,

$w_r$  – width of single rib, m,

$t_r$  – thickness of single rib, m.

Surface area of a single rib  $A_r$  can be calculated with the following equation (5.11).

$$A_r = 2\pi(r_r^2 - r_o^2), \quad (5.11)$$

where  $A_r$  – surface area of a single rib,  $m^2$ ,

$r_r$  – outer radius of rib, m,

$r_o$  – outer radius of tube, m.

Total outer surface area  $A_t$  including the ribs can be calculated with the equation (5.12).

$$A_t = \pi D_o (L_{HE} N_{tube} - t_r N_r) + A_r N_r, \quad (5.12)$$

where  $A_t$  – total outer surface area of heat exchanger,  $m^2$ ,

$D_o$  – outer diameter of tube, m,

$L_{HE}$  – Length of one tube in heat exchanger, m,

$N_{tube}$  – number of tubes in a heat exchanger,

$t_r$  – thickness of single rib, m,

$N_r$  – the total number of ribs in the heat exchanger,

$A_r$  – surface area of a single rib,  $m^2$ .

Visual representation of rib and tube dimensions were given on Figure 4.4 and Figure 4.5.

The heat transfer coefficient can then be calculated by deriving it from the equation (5.13) [21].

$$Nu_{EG} = \frac{k_h D_o}{\lambda_{EG}} \Rightarrow k_h = \frac{Nu_{EG} \lambda_{EG}}{D_o}, \quad (5.13)$$

where  $k_h$  – heat transfer coefficient between exhaust gas and heat exchanger,  $W/(m^2 \cdot K)$ ,

$Nu_{EG}$  – Nusselt number for exhaust gas,

$\lambda_{EG}$  – thermal conductivity of exhaust gas,  $W/(m \cdot K)$ ,

$D_o$  – outer diameter of tube, m.

Nusselt number,  $Nu_{EG}$ , for circular cylinder with cross-flow can be calculated with equation (5.14) [21].

$$Nu_{EG} = C_1 C_2 Re_{EG}^m Pr_{EG}^{0.36} \left( \frac{Pr_{EG}}{Pr_{EGS}} \right)^{1/2}, \quad (5.14)$$

where  $Nu_{EG}$  – Nusselt number for exhaust gas,

$C_1$  – correction constant based on the spacing of tubes in heat exchanger,

$C_2$  – correction constant based on the number of layers in heat exchanger,

$Re_{EG}$  – Reynolds number for exhaust gas,

$Pr_{EG}$  – Prandtl number for exhaust gas,

$Pr_{EGS}$  – Prandtl number for exhaust gas at the mean temperature of the tube,

$m$  – power of Reynolds number.

Correction constants  $C_1$  and  $C_2$  depend on the size of the tubes and their spacing, and are evaluated in the section where the equation (5.14) is applied. The value for the power of Reynolds number,  $m$ , depends on the Reynolds number and is evaluated also in the section where the equation is applied. In the equation (5.14) the Reynolds number is calculated based on the maximum speed of exhaust gas in the heat exchanger [21]. The maximum speed of exhaust gas in between a staggered tube bank can be either in the direction along the overall movement of the exhaust gas or diagonally between the tubes. This depends on the spacing of tubes and the maximum speed occurs along the overall exhaust gas movement if the following condition expressed with equation (5.15) is true [21].

$$2(S_D - D_o) > (S_T + D_o), \quad (5.15)$$

where  $S_D$  – aligned distance between tubes in different layers, m,

$D_o$  – outer diameter of tube, m,

$S_T$  – distance between tubes in the same layer, m.

When the condition is true, the maximum speed can be calculated with the equation (5.16) [21].

$$V_{max} = \frac{S_T}{(S_T - D_O)} V, \quad (5.16)$$

where  $V_{max}$  – maximum exhaust gas velocity, m/s,

$S_T$  – distance between tubes in the same layer, m,

$D_O$  – outer diameter of tube, m,

$V$  – average exhaust gas velocity, m/s.

The average velocity of exhaust gas can be calculated with the equation (5.17).

$$V = \frac{M_1}{\rho_{EG} A_{HE}}, \quad (5.17)$$

where  $V$  – average exhaust gas velocity, m/s,

$M_1$  – mass flow rate of exhaust gas, kg/s,

$\rho_{EG}$  – density of exhaust gas, kg/m<sup>3</sup>,

$A_{HE}$  – cross-section area of heat exchanger, m<sup>2</sup>.

Density of the exhaust gas is calculated at the average temperature of exhaust gas ( $\Delta t_{m1} = 479,4 \text{ K}$ ) and absolute pressure ( $P_{ABS} = P_i + 101\,325 \text{ Pa} = 0 + 101\,325 = 101\,325 \text{ Pa}$ ) with the equation (5.18).

$$\rho_{EG} = \frac{P_{ABS} M_{EG}}{R_u \Delta t_{m1}}, \quad (5.18)$$

where  $\rho_{EG}$  – density of exhaust gas, kg/m<sup>3</sup>,

$P_{ABS}$  – absolute pressure of exhaust gas, Pa,

$M_{EG}$  – molar mass of exhaust gas, kg/kmol,

$R_u$  – universal gas constant, 8314 J/(kmol · K),

$\Delta t_{m1}$  – average temperature of exhaust gas, K.

Reynolds number for exhaust gas flowing over circular cylinder can then be calculated with the equation (5.19) [21].

$$Re_{EG} = \frac{V_{max} D_O}{\nu_{EG}}, \quad (5.19)$$

where  $Re_{EG}$  – Reynolds number for exhaust gas,

$V_{max}$  – maximum exhaust gas velocity, m/s,

$D_O$  – outer diameter of tube, m,

$\nu_{EG}$  – kinematic viscosity of exhaust gas, m<sup>2</sup>/s.

The equations (5.8) through (5.19) are used to calculate the exhaust gas side of thermal resistance in the heat exchanger.

For calculating the thermal resistance of the tube,  $R_w$ , in the heat exchanger the equation (5.20) can be used [21].

$$R_w = \frac{\ln\left(\frac{r_o}{r_i}\right)}{2\pi L_{HE} N_{tube} \lambda_t}, \quad (5.20)$$

where  $R_w$  – thermal resistance of heat exchanging tube, W/K,

$r_o$  – outer radius of tube, m,

$r_i$  – inner radius of tube, m,

$L_{HE}$  – Length of one tube in heat exchanger, m,

$N_{tube}$  – number of tubes in a heat exchanger,

$\lambda_t$  – thermal conductivity of a tube in heat exchanger, W/(m·K).

The equation (5.20) is used for radial conduction through a cylindrical wall. This is why logarithmic function between outer and inner radius has been used [21].

The heat transfer coefficient for the water side of heat exchanger can be calculated similarly with exhaust gas side with the equation (5.13) and is expressed with equation (5.21) [21].

$$k_c = \frac{Nu_w \lambda_w}{D_i}, \quad (5.21)$$

where  $k_c$  – heat transfer coefficient between water and heat exchanger, W/(m<sup>2</sup>·K),

$Nu_w$  – Nusselt number for water,

$\lambda_w$  – thermal conductivity of water, W/(m·K),

$D_i$  – inner diameter of tube, m.

Although the heat transfer coefficient calculation is similar, the Nusselt number for water needs to be calculated with the equation (5.22) because the flow of water is along the inner surface of the tube [21].

$$Nu_w = 0,023 Re_w^{4/5} Pr_w^n, \quad (5.22)$$

where  $Nu_w$  – Nusselt number for water,

$Re_w$  – Reynolds number for water,

$Pr_w$  – Prandtl number for water,

$n$  – power for Prandtl number.

The power for Prandtl number,  $n$ , is selected based on the heating or cooling of water.  $n = 0,4$  is selected when the substance is heated and  $n = 0,3$  when the substance is cooled. For this reason,  $n = 0,4$  is used for this case. Equation (5.22) can be used when the following criteria is met [21]:

- $0,6 \lesssim Pr_w \lesssim 160$ ,
- $Re_w \gtrsim 10\,000$ ,
- $L_{HE} N_{tube} / D_i \gtrsim 10$ .

Reynolds number in a tube of uniform cross-sectional area is calculated with the equation (5.23) [21].

$$\text{Re}_W = \frac{M_2 D_I}{N_{TL} \rho_W A_{tube} \nu_W}, \quad (5.23)$$

where  $\text{Re}_W$  – Reynolds number for water,

$M_2$  – mass flow rate of water in tube, kg/s,

$D_I$  – inner diameter of tube, m,

$N_{TL}$  – number of tubes in a layer,

$\rho_W$  – density of water, kg/m<sup>3</sup>,

$A_{tube}$  – inner cross-section area of tube, m<sup>2</sup>,

$\nu_W$  – kinematic viscosity of water, m<sup>2</sup>/s.

The number of tubes in one layer is taken into consideration because of the water mass flow is divided between the tubes in a layer. Inner cross-section area of the tube can be calculated with equation (5.24).

$$A_{tube} = \pi r_i^2, \quad (5.24)$$

where  $A_{tube}$  – inner cross-section area of tube, m<sup>2</sup>,

$r_i$  – inner radius of a tube, m.

The total inner surface area is obtained with equation (5.25).

$$A_c = \pi D_I L_{HE} N_{tube}, \quad (5.25)$$

where  $A_c$  – total inner surface area, m<sup>2</sup>,

$D_I$  – inner diameter of tube, m,

$L_{HE}$  – Length of one tube in heat exchanger, m,

$N_{tube}$  – number of tubes in a heat exchanger.

By combining the needed rate of heat exchange equation (5.1) and equation (5.5), the average temperature difference between exhaust gas and water can be calculated. Thus, the actual temperature of exhaust gas at the outlet of heat exchanger evaluated by solving the equation (5.6) for the smallest temperature difference  $\Delta t_s$  and subtracting the water inlet temperature  $T_2$  from that.

# 6. QUENCHING SEGMENT REPLACEMENT EVALUATION

## 6.1 Rate of heat exchange from exhaust gas

In order to calculate the rate of heat exchange from the exhaust gas, the enthalpies and therefore the average isobaric specific heat must be calculated with equation (5.4).

$$c_{mp} \Big|_{t_2}^{t_1} = \frac{c_{p1}t_1 - c_{p2}t_2}{t_1 - t_2} = \frac{1043,3 \times 292,5 - 1027,7 \times 120}{292,5 - 120} = 1054,2 \text{ J/(kg} \cdot \text{K)}.$$

The rate of heat exchange can be calculated by combining equations (5.1), (5.2) and (5.3) giving the following equation (6.1).

$$Q = M_1 c_{mp} \Big|_{T''_1}^{T'_1} (T'_1 - T''_1) = 20,278 \cdot 1054,2(565,65 - 393,15) = 3\,687\,544 \text{ W} \quad (6.1)$$

Similarly, the rate of heat exchange can be calculated from the minimum exhaust gas inlet temperature up to maximum temperature of  $T'_1=643,15$  K and mass flow rate up to  $M_1=91000\text{kg/h} = 25,280$  kg/s. Table 6.1 shows the minimum and maximum rates of heat exchanges for the exhaust gas along with result from equation (6.1).

Table 6.1 Rates of heat exchange for exhaust gas

| Inlet temperature, $T'_1$ , K | Outlet temperature, $T''_1$ | Mass flow rate, $M_1$ , kg/s | Rate of heat exchange, $Q$ , W |
|-------------------------------|-----------------------------|------------------------------|--------------------------------|
| 488,15                        | 393,15                      | 20,278                       | 2014350                        |
| 565,65                        | 393,15                      | 20,278                       | 3687589                        |
| 643,15                        | 393,15                      | 25,278                       | 6720088                        |

## 6.2 Heat exchanger evaluation

Input information for heat exchanger evaluation is taken from tables in chapter 4. The heat exchanger properties are evaluated based on the initial dimensions and properties given by Clean Marine and then altered if higher rate of heat exchange is needed.

### 6.2.1 Thermal resistance of exhaust gas

For evaluating the thermal resistance of exhaust gas in heat exchanger, the region of maximum velocity must be determined. Using the equation (5.15) the maximum velocity is determined to be in alignment with the exhaust gas overall movement.

$$2(S_D - D_O) = 2(0,05 - 0,028) = 0,044 > 0,022 = (0,05 - 0,028) = (S_T - D_O).$$

Using the equation (5.18) the density of exhaust gas is determined.

$$\rho_{EG} = \frac{P_{ABS} M_{EG}}{R_u \Delta t_{m1}} = \frac{101325 \times 28,82}{8314 \times 479,4} = 0,733 \text{ kg/m}^3.$$

Equation (5.17) can be used to determine the average velocity of exhaust gas through the heat exchanger.

$$V = \frac{M_1}{\rho_{EG} A_{HE}} = \frac{20,278}{0,733 \cdot 1,6} = 17,29 \text{ m/s.}$$

The maximum velocity of exhaust gas is calculated with equation (5.16).

$$V_{max} = \frac{S_T}{(S_T - D_O)} V = \frac{0,05}{(0,05 - 0,028)} 17,29 = 39,30 \text{ m/s.}$$

With the maximum velocity known, Reynolds number is calculated with equation (5.19).

$$Re_{EG} = \frac{V_{max} D_O}{\nu_{EG}} = \frac{39,30 \cdot 0,028}{3,36 \cdot 10^{-5}} = 32\,750.$$

Calculating the Nusselt number with equation (5.14) for exhaust gas requires the correction constants and a power for Reynolds number. The correction constant  $C_1$  can be calculated with the equation (6.2) and the power of Reynolds number is  $m = 0,6$  based on the staggered tube bank geometry and the condition of  $10^3 \lesssim Re_{EG} = 32\,750 \lesssim 2 \times 10^5$  [21].

$$C_1 = 0,35 \left( \frac{S_T}{S_L} \right)^{1/5} = 0,35 \left( \frac{0,05}{0,0433} \right)^{1/5} = 0,36. \quad (6.2)$$

The correction constant  $C_2=1$  due to the number of layers in the staggered heat exchanger  $N_{layer} = 55$  [21]. This gives the final form to equation (5.14) for calculating Nusselt number.

$$Nu_{EG} = C_1 C_2 Re_{EG}^m Pr_{EG}^{0,36} \left( \frac{Pr_{EG}}{Pr_{EGS}} \right)^{1/2} = 0,36 \times 1 \times 32\,750^{0,6} \times 0,65^{0,36} \left( \frac{0,65}{0,69} \right)^{1/2} = 153,15.$$

The heat transfer coefficient on the exhaust gas side can then be calculated with the equation (5.13).

$$Nu_{EG} = \frac{k_h D_O}{\lambda_{EG}} \Rightarrow k_h = \frac{Nu_{EG} \lambda_{EG}}{D_O} = \frac{153,15 \times 0,041}{0,028} = 224,26 \text{ W/(m}^2 \cdot \text{K)}.$$

Next to be determined is the overall efficiency of the surface on the exhaust gas side. Using the equation (5.10), the efficiency of a single rib can be calculated.

$$\eta_r = \frac{\tanh \left[ \sqrt{\frac{2k_h}{\lambda_t t_r w_r}} \cdot \left( w_r + \frac{t_r}{2} \right)^{3/2} \right]}{\sqrt{\frac{2k_h}{\lambda_t t_r w_r}} \cdot \left( w_r + \frac{t_r}{2} \right)^{3/2}} = \frac{\tanh \left[ \sqrt{\frac{2 \times 224,26}{16 \times 0,002 \times 0,011}} \cdot \left( 0,011 + \frac{0,002}{2} \right)^{3/2} \right]}{\sqrt{\frac{2 \times 224,26}{16 \times 0,002 \times 0,011}} \cdot \left( 0,011 + \frac{0,002}{2} \right)^{3/2}} = 0,608.$$

For calculating the overall efficiency of the outer surface, the surface areas of all the ribs and total outer surface area must be calculated. Therefore, the number of ribs per single tube must be calculated with the equation (6.3).

$$N_{rpt} = \frac{L_{EH}}{S_r} = \frac{1,265}{0,004} = 316,25 \approx 316, \quad (6.3)$$

where  $N_{rpt}$  – number of ribs per single tube.

This gives the total number of ribs with the equation (6.4).

$$N_r = N_{tube} \times N_{rpt} = 1375 \times 316 = 434\,500 \quad (6.4)$$

The surface area of a single rib is calculated with the equation (5.11).

$$A_r = 2\pi(r_r^2 - r_o^2) = 2\pi(0,025^2 - 0,014^2) = 2,70 \times 10^{-3} \text{ m}^2.$$

The total surface area on the side of exhaust gas can then be calculated with the equation (5.12).

$$\begin{aligned} A_t &= \pi D_o(L_{HE} \cdot N_{tube} - t_r N_r) + A_r \cdot N_r = \\ &= \pi \times 0,028(1,265 \times 1375 - 0,002 \times 434\,500) + 2,70 \times 10^{-3} \times 434\,500 = \\ &= 1249,7 \text{ m}^2. \end{aligned}$$

The total surface efficiency is then calculated with the equation (5.8).

$$\eta_0 = 1 - \frac{N_r A_r}{A_t} (1 - \eta_r) = 1 - \frac{434\,500 \times 2,70 \times 10^{-3}}{1249,7} (1 - 0,608) = 0,632.$$

With the overall surface efficiency of  $\eta_0 = 0,632$ , total outer surface area of  $A_t = 1249,7 \text{ m}^2$  and the heat transfer coefficient of  $k_h = 224,26 \text{ W}/(\text{m}^2 \cdot \text{K})$ , the overall thermal resistance on the side of exhaust gas can be calculated with the equation (6.5) based on the equation (5.7).

$$R_{EG} = \frac{1}{\eta_0 k_h A_t} = \frac{1}{0,608 \times 224,26 \times 1249,7} = 5,86 \times 10^{-6} \text{ K/W}, \quad (6.5)$$

where  $R_{EG}$  – thermal resistance between exhaust gas and heat exchanger K/W.

As seen from the equation (6.5), one significant factor is the overall surface efficiency. Further optimising is done when the initial heat exchanger properties are calculated.

### 6.2.2 Thermal resistance of tubes in heat exchanger

The overall thermal resistance of tubes in heat exchanger is calculated with the equation (5.20).

$$R_w = \frac{\ln\left(\frac{r_o}{r_i}\right)}{2\pi L_{HE} N_{tube} \lambda_t} = \frac{\ln\left(\frac{0,014}{0,012}\right)}{2\pi \times 1,265 \times 1375 \times 16,0} = 8,82 \times 10^{-7} \text{ K/W}.$$

### 6.2.3 Thermal resistance of water in heat exchanger

Based on the properties of water from Table 4.3 and the rate of heat exchange ( $Q = 3\,687\,544 \text{ W}$ ) from equation (6.1), the mass flow rate of water can be calculated with equation (5.1) solving for  $M_2$ .



$$Q = M_2(h''_2 - h'_2) \Rightarrow M_2 = \frac{Q}{h''_2 - h'_2} = \frac{3\,687\,544}{2\,833\,207 - 461\,368} = 1,55 \text{ kg/s.}$$

For calculating Reynolds number, the inner cross-section area  $A_{tube}$  is calculated with equation (5.24).

$$A_{tube} = \pi r_I^2 = \pi \times 0,012^2 = 4,52 \times 10^{-4} \text{ m}^2.$$

The Reynolds number can then be calculated using the equation (5.23) with water mass flow rate of  $M_2 = 1,55 \text{ kg/s}$  and  $A_{tube} = 4,52 \times 10^{-4} \text{ m}^2$ .

$$Re_W = \frac{M_2 D_I}{N_{TL} \rho_W A_{tube} v_W} = \frac{1,55 \times 0,024}{25 \times 0,788 \times 4,52 \times 10^{-4} \times 1,77 \times 10^{-5}} = 236\,029.$$

The Nusselt number for water can then be calculated with the equation (5.22) given that the following criteria is met:

- $0,6 \lesssim Pr_W = 0,994 \lesssim 160$ ,
- $Re_W = 236\,029 \gtrsim 10\,000$ ,
- $L_{HE} N_{tube} / D_I = \frac{1,265 \times 1375}{0,024} = 72\,473,0 \gtrsim 10$ .

$$Nu_W = 0,023 Re_W^{4/5} Pr_W^n = 0,023 \times 236\,029^{4/5} \times 0,994^{0,4} = 456,1.$$

The heat transfer coefficient is then calculated with the equation (5.21).

$$k_c = \frac{Nu_W \lambda_W}{D_I} = \frac{456,1 \times 0,0285}{0,024} = 541,6 \text{ W/(m}^2 \cdot \text{K)}.$$

The total inner (water side) surface area  $A_c$  can be calculated with the equation (5.25).

$$A_c = \pi D_I L_{HE} N_{tube} = \pi \times 0,024 \times 1,265 \times 1375 = 131,15 \text{ m}^2.$$

The total inner surface thermal resistance,  $R_I$ , can then be calculated with equation (6.6) based on the equation (5.7).

$$R_I = \frac{1}{k_c A_c} = \frac{1}{541,6 \times 131,15} = 1,408 \times 10^{-5} \text{ K/W}, \quad (6.6)$$

where  $R_I$  – total inner surface thermal resistance, K/W.

#### 6.2.4 Exhaust gas temperature at the outlet of heat exchanger

The mean temperature difference between exhaust gas and water is calculated with the equation (5.6) based on the initial temperatures.

$$\Delta t_m = \frac{\Delta t_l - \Delta t_s}{\ln \frac{\Delta t_l}{\Delta t_s}} = \frac{(T'_1 - T''_2) - (T''_1 - T'_2)}{\ln \left[ \frac{(T'_1 - T''_2)}{(T''_1 - T'_2)} \right]} = \frac{(565,65 - 453,15) - (393,15 - 383,15)}{\ln \left[ \frac{(565,65 - 453,15)}{(393,15 - 383,15)} \right]} = 42,35 \text{ K.}$$

As the thermal resistances of exhaust gas, tubes and water are known, the mean temperature difference can be calculated based on the geometry of heat exchanger and needed rate of heat exchange by solving equation (5.5) for  $\Delta t_m$ .

$$\begin{aligned} \Delta t_{m,HE} &= QR = Q(R_{EG} + R_W + R_I) = 3\,687\,544(5,86 \times 10^{-6} + 8,82 \times 10^{-7} + 1,408 \times 10^{-5}) \\ &= 76,78 \text{ K,} \end{aligned}$$

where  $\Delta t_{m,HE}$  – the mean temperature difference between exhaust gas and water based on heat exchanger calculations, K.

As seen from above calculations  $\Delta t_m \neq \Delta t_{m,HE}$  which means the actual exhaust gas outlet temperature is higher than  $T''_1 = 393,15$  K for this heat exchanger. By solving calculation (5.6) for  $\Delta t_s$ , the smallest temperature difference between exhaust gas and water be evaluated [25].

$$\Delta t_m = \frac{\Delta t_l - \Delta t_s}{\ln \frac{\Delta t_l}{\Delta t_s}} \Rightarrow \Delta t_s = 49,55 \text{ K.}$$

As the smallest temperature difference in this case occurs at the outlet of the heat exchanger, the exhaust gas temperature can be calculated with equation (6.7).

$$T''_1 = T'_2 - \Delta t_s = 383,15 + 49,55 = 432,70 \text{ K.} \quad (6.7)$$

Given that the initial exhaust gas temperature at the outlet was proposed lower than calculations show, the actual thermal resistance is lower than calculated. After calculating the overall thermal resistance again, the actual exhaust gas outlet temperature for this configuration of heat exchanger is  $T''_1 = 422,75$  K with a 2% error in value compared to equation (6.7). As the equations to evaluate the heat exchanger could have an error based on literature, in calculating the heat transfer coefficients, of up to 20%, the difference in actual exhaust gas temperature and value from (6.7) is insignificant [23]. For this reason, further optimisation calculations do not account for these minor errors and exhaust gas temperature is calculated based on equation (6.7).

### 6.3 Optimising the heat exchanger

For the exhaust gas inlet temperature of  $T'_1 = 565,65$  K and desired exhaust gas outlet temperature of  $T''_1 = 393,15$  K, the optimisation of heat exchanger is done by altering geometric dimensions such as tube diameter, rib thickness, rib spacing and rib diameter. For any optimisation calculation, all the equations from chapter 6.2 are calculated again. Exhaust gas outlet temperatures dependent on the tube diameter are shown in Figure 6.1.

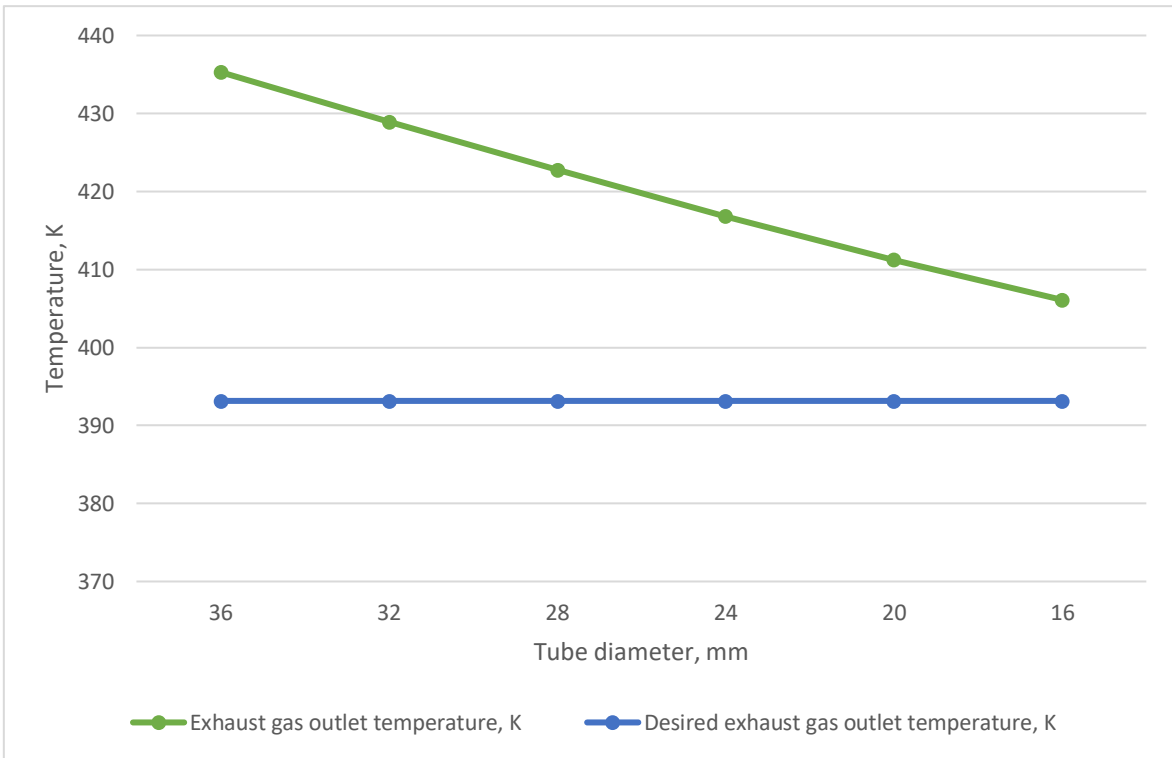


Figure 6.1 Actual exhaust gas temperatures dependent on the tube diameter

As seen on Figure 6.1, the decrease in tube diameter significantly lowers the actual exhaust gas temperature with the lowest value of  $T''_i=406,1$  K at  $D_o=16$  mm. Further adjustment to geometry is made by fixing the tube diameter to  $D_o=16$  mm. Figure 6.2 shows the impact of rib thickness and rib spacing to the exhaust gas outlet temperature.

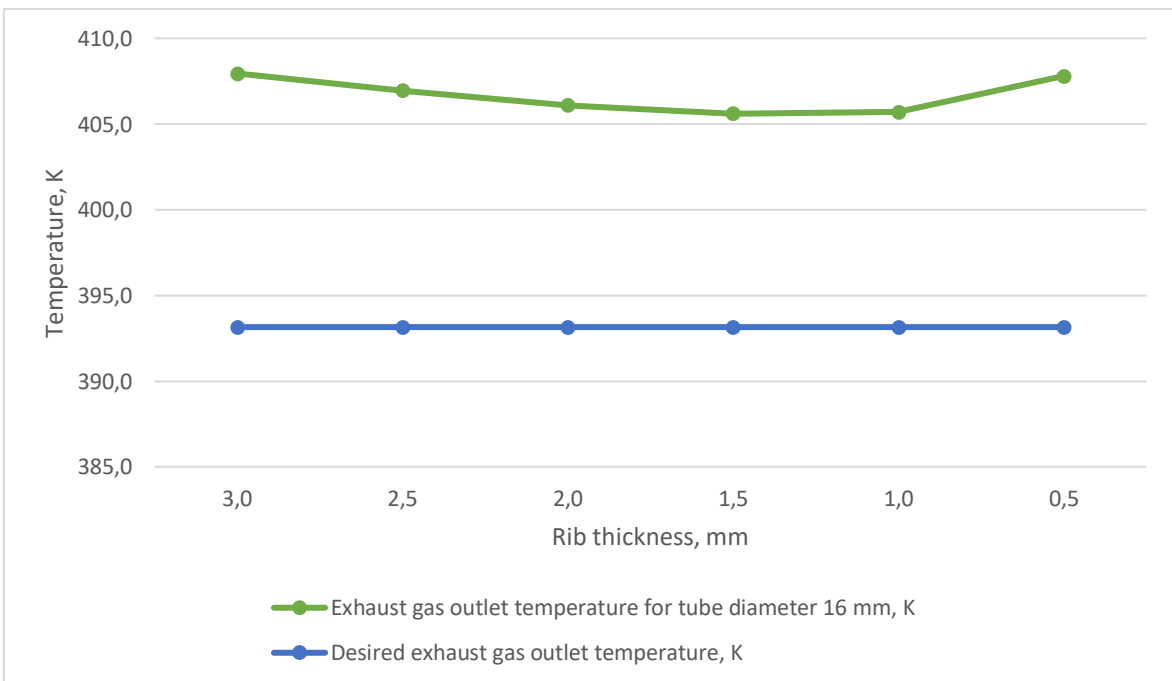


Figure 6.2 Rib thickness impact on exhaust gas temperature for tube diameter of 16 mm

No significant improvement in changing the rib thickness for  $D_o=16$  mm is noted. Furthermore, with thinner rib thickness than 1,5 mm, the calculated exhaust gas temperature raises. This is caused by the faster decrease in surface efficiency than increase in surface area. Figure 6.3 shows the impact of rib spacing to the exhaust gas outlet temperature. Rib thickness of  $t_r=1,5$  mm and tube diameter of  $D_o=16$  mm is chosen for this.

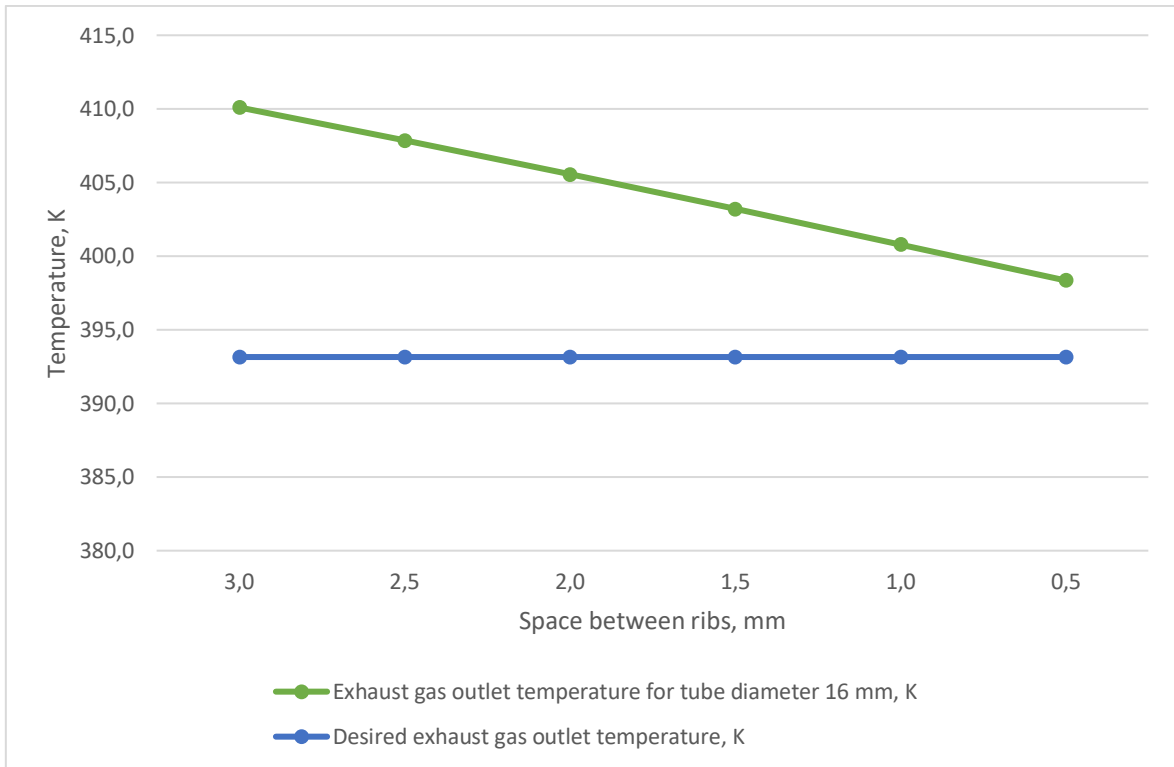


Figure 6.3 Rib spacing impact on exhaust gas outlet temperature, for  $D_o=16$  mm and  $t_r=1,5$  mm

As seen from Figure 6.3 the exhaust gas temperature is falling almost linearly by decreasing the space between ribs. The best result is achieved with minimum space between the ribs due to increased surface area on the exhaust gas side. Figure 6.4 shows the impact of rib diameter on the exhaust gas outlet temperature with  $t_r=1,5$  mm and  $S_r=2$  mm (space between ribs is therefore 0,5 mm). Significant decrease in exhaust gas temperatures is observed with decreasing the diameter of the rib. Minimum exhaust gas temperature achieved was  $T''_1=388,6$  K which is lower than the desired outlet temperature. As the  $T''_1$  is still higher than water inlet temperature of  $T'_2=383,15$  K, the criteria to lower the exhaust gas temperature to desired value was achieved.

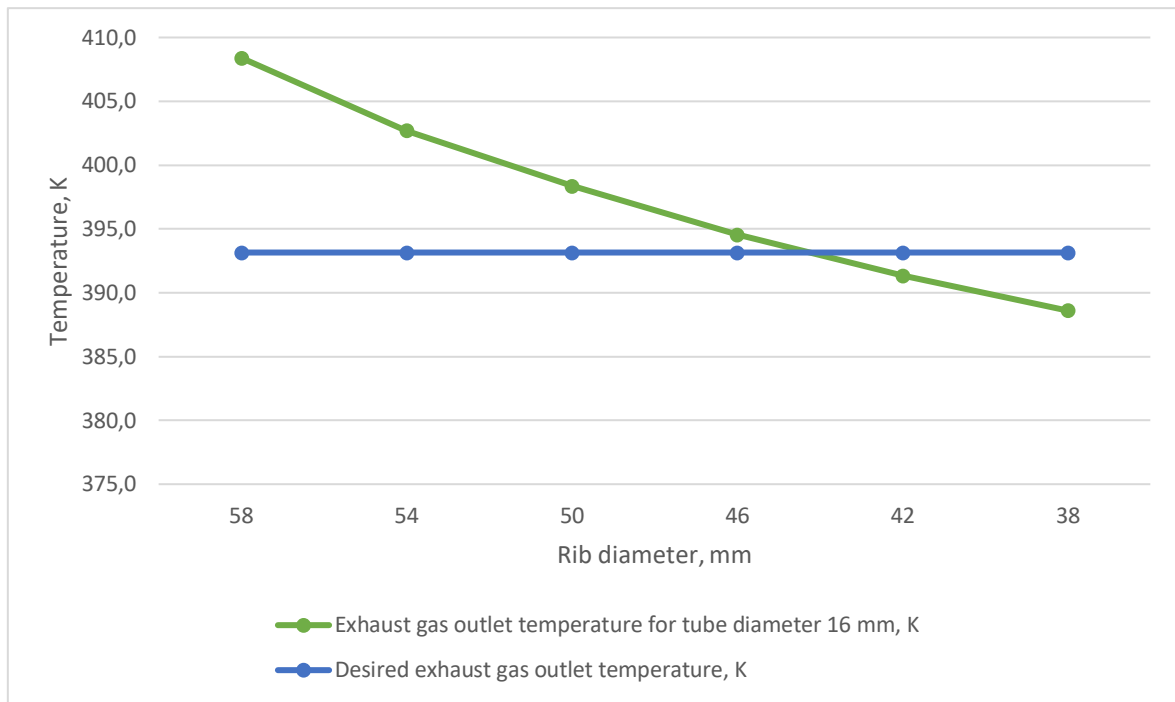


Figure 6.4 Impact of rib diameter on exhaust gas outlet temperature

Although Figure 6.2 indicates that thinner rib thickness than 1,5 mm are counterproductive, with smaller space than 2 mm between ribs the decrease in exhaust gas temperature is still observed. By calculating the tube and rib dimensions also for the minimum and maximum exhaust gas inlet temperatures (Table 6.1) to heat exchanger, the optimum dimensions are shown in Table 6.2.

Table 6.2 Optimum tube and rib dimensions for different conditions

|   | <b>Minimum condition</b> | <b>Average condition</b> | <b>Maximum condition</b> |
|---|--------------------------|--------------------------|--------------------------|
| Inlet temperature, $T'_1$ , K           | 488,15                   | 565,65                   | 643,15                   |
| Desired outlet temperature, $T''_1$ , K | 393,15                   | 393,15                   | 393,15                   |
| Mass flow rate, $M_1$ , kg/s            | 20,278                   | 20,278                   | 25,278                   |
| Tube diameter, $D_o$ , mm               | 16                       | 16                       | 16                       |
| Rib thickness, $t_r$ , mm               | 1                        | 1                        | 1                        |
| Rib spacing, $S_r$ , mm                 | 2                        | 2                        | 2                        |
| Rib diameter, $D_r$ , mm                | 38                       | 38                       | 38                       |
| Actual outlet temperature, $T''_1$ , K  | 401,6                    | 389,2                    | 387,5                    |

As Table 6.2 indicates, at the minimum conditions, the heat exchanger would still need to cool the exhaust gas by 8,5 K. Calculations show that the lowest exhaust gas inlet temperature of 500 K is the limit at which the heat exchanger can manage to cool the exhaust gas to at least 393,15 K. Since this difference compared to the minimum conditions is relatively small, it was considered negligible.

## 6.4 Properties of TEG system

The investigated TEG unit within TEG system has highly proprietary information about the  $ZT$  values and efficiencies. Thus, in depth discussion on the properties of TEG unit is not done [17]. Obtainable information regarding the TEG unit was the output power based on the parameters of water at the inlet and outlet of heat exchanger. These values are shown in Table 6.3.

Table 6.3 Power output of TEG unit [17]

| Parameter   | Unit | Value             |
|---|------|-------------------|
| Water pressure, $P_W$                                 | Pa   | $1,5 \times 10^5$ |
| Water inlet temperature to heat exchanger, $T'_2$     | K    | 383,15            |
| Water outlet temperature from heat exchanger, $T''_2$ | K    | 453,15            |
| Water mass flow rate, $M_2$                           | kg/s | 0,8 – 3           |
| Power output of TEG unit, $P_{TEG}$                   | kW   | $\geq 60$         |

The water inlet and outlet temperatures of heat exchanger are the water outlet and inlet temperatures of the TEG unit, respectively. Important to note about the TEG output power is that the power needed to operate the TEG system itself is already considered and the given output power is the net value of usable power from TEG system. This also includes the pressure drop on the water side of the heat exchanger.

## 7. ECONOMIC EVALUATION OF REPLACING QUENCHING SEGMENT WITH TEG SYSTEM

The financial calculations were done based on the extent of quenching segment replacement possibility. Since calculations show that at most of the operating conditions, the heat exchanger is sufficient to cool the exhaust gas to desired temperature, the replacement of whole quenching segment is considered.

### 7.1 Power gain on integrating TEG system

In order to evaluate the total power gain by integrating TEG system, other power losses and gains were considered. On the side of exhaust gas, the power loss is due to the pressure drop of exhaust gas passing through the heat exchanger. Based on the heat exchanger dimensions, the estimated pressure drop was  $\Delta p_{EG} = 1$  kPa approximately [17]. As seen from Figure 4.2 the gauge pressure of exhaust gas after quenching can be lower than 0 Pa down to -130 Pa. This in turn means, that the current pressure drop can be subtracted from the pressure drop initiated by heat exchanger. The average of those numbers is considered in calculating the overall power loss. The power loss is then expressed with equation (7.1) based on the average conditions of scrubbing process.

$$\begin{aligned} P_{loss,EG} &= (\Delta p_{EG} - \Delta p_{QS}) \times M_1 \times \rho_{EG} = (1000 - 65) \times 20,278 \times 0,733 = 13\,897 \text{ W} = \\ &= 13,897 \text{ kW}, \end{aligned} \quad (7.1)$$

where  $P_{loss,EG}$  – Power loss due to pressure drop on exhaust gas side, W,  
 $\Delta p_{EG}$  – pressure drop of exhaust gas passing through heat exchanger, Pa,  
 $\Delta p_{QS}$  – average pressure drop during quenching, Pa.

Based on given information, the recirculation fan operates usually at around 85 % of its rated power of 120 kW [17]. This is enough to compensate for the occurring pressure drop in heat exchanger.

Since less seawater is then sprayed due to the absence of quenching segment, the power gain of seawater pump is considered. As approximately 10 % of scrubbing water is currently used in quenching and the seawater in that segment is sprayed at higher pressure than in the rest of the scrubber, a conservative assumption is made that power gain on seawater pump is around 10%. The seawater pump's rated power is 120 kW with the average load of 85% [17]. The power gain on seawater pump is therefore calculated with equation (7.2).

$$P_{gain,SWP} = P_{SWP} \times 0,85 \times 0,1 = 120 \times 10^3 \times 0,85 \times 0,1 = 10\,200 \text{ W} = 10,2 \text{ kW}, \quad (7.2)$$

where  $P_{gain,SWP}$  – power gain on seawater pump, W,

$P_{SWP}$  – rated power of seawater pump, W.

The total usable power is then calculated with equation (7.3).

$$\begin{aligned} P_{total} &= P_{TEG} + P_{gain,SWP} - P_{loss,EG} = 60 \times 10^3 + 10,2 \times 10^3 - 13,897 \times 10^3 = 56\,303 \text{ W} = \\ &= 56,303 \text{ kW}. \end{aligned} \quad (7.3)$$

## 7.2 Reduced cost of building the wet scrubber compared to current version

Instant savings on the building phase of the wet scrubber come from the reduced material used. Since the quenching segment of the scrubber is in more extreme environment than the rest of the scrubber, more durable material must be used. This in turn means the quenching segment by material is one of the most expensive parts of the scrubber. Cost of manufacturing the quenching segment can be divided into two: cost of material and cost of manufacturing. The material includes sheet metal, tubes and tube fittings. The manufacturing includes welding, bending, rolling and surface treatments. The sum of costs to manufacture quenching segment is the instant savings from integrating TEG system, seen in Table 4.7. The evaluation of replacement possibility resulted that the whole segment could be replaced. This gives the total amount of instant savings from manufacturing as  $C_{mf}=16\,280,32 \text{ €}$ .

## 7.3 Financial calculations

Evaluating the economic justification, five aspects are considered: investments into integrating TEG, reduced cost from manufacturing compared to the current version of wet scrubber, the financial return period, NPV and IRR.

Financial return period depends on the investment and the reduction of operating costs. The reduction on operating costs comes solely from the consumption of Marine diesel oil (MDO) for auxiliary diesel engines since these are the only electric power sources on the vessel before the installation of TEG. The fuel reduction depends on how much MDO was needed for achieving the same amount of electric energy compared to what TEG would produce. The prices and values shown in Table 7.1 were obtained from Clean Marine AS based on their information as of February 2020 [17].



Table 7.1 Information about TEG system, investment and electricity [17]

| <b>TEG and Electricity information</b>      | <b>Unit</b>    | <b>Value</b>   |
|---|----------------|----------------|
| Price of TEG system, $PR_{TEG}$             | €              | 246 310        |
| Operation time, $OT$                        | h/year         | 7800           |
| Price of marine diesel oil (MDO), $P_{MDO}$ | €/t (€/kg)     | 599,05 (0,599) |
| Consumption of MDO, $Q_{MDO}$               | kg/kWh (kg/GJ) | 0,23 (63,89)   |
| Investment period, $I_0$                    | years          | 10             |
| Price of electricity, $PR_E$                | €/kWh (€/GJ)   | 0,14 (38,27)   |

The price of electricity generated on board of a vessel currently with auxiliary engines was calculated with the equation (7.4).

$$PR_E = P_{MDO} \times Q_{MDO} \times 3,6 \times 10^{-3} = 0,599 \times 63,89 \times 3,6 \times 10^{-3} = 38,27 \text{ €/GJ (0,14 €/kWh)} \quad (7.4)$$

As mentioned, the TEG output power of  $P_{TEG} > 60$  kW is the net value (operational need subtracted). The annual savings are calculated with the equation (7.5) based on the result of equation (7.3) and information from Table 7.1.

$$a = P_{total} \cdot OT \cdot PR_E = 56,303 \times 7800 \times 0,14 = 61\,483 \text{ €/year,} \quad (7.5)$$

where  $a$  – annual savings from operation costs, €/year,

$P_{total}$  – total power gain from integrating TEG system, kW,

$OT$  – operation time of vessel, h/year,

$PR_E$  – price of electricity produced currently with MDO, €/kWh (€/GJ).

The financial return period can then be calculated with the following equation (7.6).

$$FRP = \frac{I_0 - C_{mf}}{a} = \frac{246\,310 - 16\,280,32}{61\,483} = 3,7 \text{ years,} \quad (7.6)$$

where FRP – financial return period, years,

$I_0$  – investment into TEG system, €,

$C_{mf}$  – manufacturing cost of quenching segment,

$a$  – annual savings from operation costs, €/year.

The financial sustainability can be further analysed by calculating the IRR and NPV. Both, NPV and IRR are calculated with Microsoft Excel and are shown in Table 8.2 along with the overview of other financial indicators.

## SUMMARY

The waste heat and CO<sub>2</sub> in quantity have been rising for the last decades with more contributing factor over time being the maritime industry [1]–[3]. Thus, the possibility of using some of the waste heat to convert directly into electrical energy was investigated.

In this thesis the overview of the thermoelectric materials and thermoelectric generators (TEGs) along with applications was given. Many of the thermoelectric materials studied and improved to this day have already been discovered decades ago. Most improvement has been noticed by doping the materials with substituting some of the atoms to enhance the electrical conductivity and decrease the thermal conductivity. Thermoelectric generators have been used initially on spacecrafts but as the materials and technology developed, more fields of applications have found use in TEGs. This includes using TEG in extreme environments, waste heat recovery, decentralized domestic power applications, micro-generation for microelectronics and solar thermoelectric generators.

With the current exhaust gas cleaning systems on vessels, the concentration of gaseous pollutants and particulate matter are removed or reduced to satisfactory level in comparison to the set limits [26]. Along with other exhaust gas cleaning systems (dry scrubbers, selective catalytic reduction, and exhaust gas recirculation) wet scrubber was investigated in this study, which is targeted to lower the SO<sub>x</sub> and particulate matter concentration in exhaust gas.

The first zone at which the scrubbing process begins, is the rapid cooling of exhaust gas called quenching. The quenching reduces the heat of exhaust gas vastly in preparation for the scrubbing zone. This part of the scrubber was analysed to be replaced by the TEG system as the manufacturing cost of the quenching segment is expensive relative to its mass compared to the rest of the scrubber. The TEG system in this case uses heat exchanger to transfer heat from a source to the TEG unit. The geometrical parameters of heat exchanger were calculated to lower the exhaust gas temperature to desired temperature. After initial calculations and further optimisations, the conclusion was made that the heat exchanger could replace the quenching segment entirely. The results of the calculations are shown in Table 8.1.

Table 8.1 Exhaust gas inlet temperatures, desired outlet temperatures and corresponding outlet temperatures from heat exchanger

| <b>Parameters</b>                          | <b>Minimum condition</b> | <b>Average condition</b> | <b>Maximum condition</b> |
|--|--------------------------|--------------------------|--------------------------|
| Exhaust gas inlet temperature, $T'_{1,}$ K | 488,15                   | 565,65                   | 643,15                   |
| Desired outlet temperature, $T''_{1,}$ K   | 393,15                   | 393,15                   | 393,15                   |
| Achieved outlet temperature, $T''_{1,}$ K  | 401,6                    | 389,2                    | 387,5                    |

Given the possibility of integrating the TEG system to scrubber, the financial calculations were done and can be seen in Table 8.2.

Table 8.2 Financial indicators for investing in the integration of TEG system to scrubber

| <b>Financial indicator</b>            | <b>Value</b> |
|---------------------------------------|--------------|
| Annual savings, $a,$ €/year           | 61 483       |
| Financial return period, $FRP,$ years | 3,7          |
| Investment period, $I_0,$ years       | 10           |
| Discount rate, %                      | 10 % [27]    |
| $NPV,$ €                              | 147 756,74   |
| $IRR,$ %                              | 23 %         |

Although the investment period is set to 10 years, TEG systems can operate up to couple of decades [6].

The realisation of replacing quenching segment with TEG system needs further and in-depth calculations on fouling and possible corrosion over time, although the selected material is of acid proof stainless steel. Although from the perspective of heat exchange, the replacement is possible, further investigation should be considered regarding the nature of cooling the exhaust gas. This is due to the difference in adiabatic cooling that is occurring currently compared to extracting heat with heat exchanger. Furthermore, more accurate results regarding annual savings and other financial indicators could be done by analysing the occurring pressure drops in depth.

# KOKKUVÕTE

Jääksoojuse ja CO<sub>2</sub> kogused on viimaste aastakümnete jooksul pidevalt tõusnud. Seejuures on üha suurema osakaalu moodustamas merendus [1]–[3]. Seetõttu on töös uuritud jääksoojuse kasutamist laeval selliselt, et väljund oleks otsene elektrienergia.

Töös on antud ülevaade termoelektrilistest materjalidest ja termoelektrilistest generaatoritest (TEG) koos nende kasutusalaadega. Paljud tänaseni uuritavad materjalid olid juba avastatud mitmeid kümnendeid tagasi. Termoelektrilistele materjalidele molekulides erinevate omadustega aatomite välja vahetamine on andnud seejuures suurima efekti, tõstes elektrijuhtivust ja langetades soojusjuhtivust. Algselt leidsid TEG-id kasutust peamiselt kosmoselaevadel, kuid materjalide ja tehnoloogia täiustumisel on TEG leidnud kasutust erinevates sektorites. Praeguse seisuga kasutatakse TEG-e nii ekstreemsetes keskkondades, jääksoojuse kasutamiseks, väheasustatud piirkondades, mikro-generaatorites mikroelektronika tarbeks, kui ka päikese soojuse genereerimisel elektrienergiaks.

Praeguste suitsugaaside puhastussüsteemidega suudetakse tagada heitgaasides sisalduvate saasteainete vähendamine või elimineerimine piisaval tasemel vastavalt seatud normidele [26]. Töös kirjeldatud suitsugaaside puhastussüsteemidest (kuiv suitsugaaside pesur, katalüütiline redutseerimine ja suitsugaaside retsirkuleerimine) on märg suitsugaaside pesurit uuritud, mis eraldab suitsugaasist vääveloksiide ja tahkeid osakesi.

Uuritud suitsugaaside pesuri esimene osa on suitsugaaside kiireloomuline jahutamine. Selles protsessis eraldatakse suur osa suitsugaaside soojusest tagamaks piisavalt madala temperatuuri, et järgmises etapis eraldada vääveloksiidid ja tahked osakesed. Uurimistöö seisnes skraberite esimest protsessi hõlmava osa väljavahetamise võimaluse uurimises TEG süsteemi vastu. Selle tingis asjaolu, et skraberite kiirjahutusprotsessis kasutatavad materjalid ja valmistus on võrreldes selle massi ja ülejäänud skraberiga kallis. Antud juhul oli TEG-i sisendtemperatuuri saavutamiseks suitsugaaside voolu paigaldatud soojusvaheti. Töös on arvatud suitsugaaside soojusvahetist lahkumise temperatuurid vastavalt soojusvaheti geomeetria, mida võrreldi vajalike suitsugaaside temperatuuridega säilitamiseks skraberite efektiivsuse. Esialgsete tulemuste põhjal soojusvahetit optimeeriti, et tagada piisav soojusülekanne suitsugaasidelt veele. Töö tulemuseks on järeldus, et skraberite esimest protsessi on võimalik asendada soojusvahetiga, mis läbi soojuskandja (vee) on sisendiks TEG-ile genereerimaks elektrienergiat. Lõplikud tulemused arvutustest on toodud allolevas tabelis (Tabel 8.1).

Tabel 8.1 Soojusvahetist väljuvate suitsugaaside temperatuurid vastavalt suitsugaaside sisenemistemperatuuridele ja vajalikele väljumistemperatuuridele

| <b>Parameeter</b>   | <b>Miinum koormus</b> | <b>Keskmine koormus</b> | <b>Maksimum koormus</b> |
|---|-----------------------|-------------------------|-------------------------|
| Suitsugaasi sisenemistemperatuur, $T'_1$ , K                              | 488,15                | 565,65                  | 643,15                  |
| Vajalik väljumistemperatuur, $T''_1$ , K                                  | 393,15                | 393,15                  | 393,15                  |
| Arvutatud suitsugaaside väljumistemperatuurid soojusvahetist, $T''_1$ , K | 401,6                 | 389,2                   | 387,5                   |

Tulenevalt võimalusest välja vahetada kogu kiirjahutusega seotud osa skraberist, arvutati majanduslikud näitajad, mis on toodud allolevas tabelis (Tabel 8.2).

Tabel 8.2 Majanduslikud näitajad investeerides TEG süsteemi integreerimisse

| <b>Majanduslik näitaja</b>      | <b>Väärtus</b> |
|---------------------------------|----------------|
| Aastane kokkuvõide, $a$ , €/a   | 61 483         |
| Lihttasuvusaeg, $FRP$ , a       | 3,7            |
| Investeeringuperiood, $I_0$ , a | 10             |
| Diskonteerimismäär, %           | 10 % [27]      |
| Nüüdispuhasväärtus, $NPV$ , €   | 147 756,74     |
| Kapitalitootlikkus, $IRR$ , %   | 23 %           |

Kuigi investeeringuperioodiks on valitud 10 aastat, siis tegelikkuses kestavad TEG süsteemid kuni 30 aastat, mis omakorda tõstab investeeringu tootlikkust.

Realiseerimaks skraberite kiirjahutusprotsessi väljavahetamist TEG süsteemi vastu, tuleks põhjalikumalt uurida pikaajalisemat mõju ummistuste ja korrosiooni vastu soojusvahetis, olenemata asjaolust, et materjaliks oli valitud happekindel roostevaba teras. Kuigi soojusülekanne vaatenurgast on jahutussüsteemi vahetamine TEG süsteemi vastu võimalik, tuleks uurida jahutamise olemuste erinevust. Erinevus seisneb selles, et kiirjahutamine praeguses süsteemis toimub adiabaatilisel, kuid uuritud soojusülekanne soojusvahetile mitte. Lisaks on võimalik täpsemalt arvutada majanduslikud näitajad analüüsid põhjalikumalt rõhulangu mõju.

## LIST OF REFERENCES

- [1] Q. Bian, "Waste heat : the dominating root cause of current global warming," *Environ. Syst. Res.*, 2020.
- [2] A. Firth, B. Zhang, and A. Yang, "Quantification of global waste heat and its environmental effects," *Appl. Energy*, vol. 235, no. October 2018, pp. 1314–1334, 2019.
- [3] M. Gallo, L. Moreschi, M. Mazzoccoli, V. Marotta, and A. Del Borghi, "Sustainability in Maritime Sector: Waste Management Alternatives Evaluated in a Circular Carbon Economy Perspective," *Resources*, vol. 9, no. 4, p. 41, Apr. 2020.
- [4] D. Gregory and N. Confuorto, "A practical guide to exhaust gas cleaning systems for the maritime industry," *EGCSA Handbook, London UK*, 2012.
- [5] C. Gayner and K. K. Kar, "Recent advances in thermoelectric materials," *Progress in Materials Science*. 2016.
- [6] D. Champier, "Thermoelectric generators: A review of applications," *Energy Conversion and Management*. 2017.
- [7] D. Beretta *et al.*, "Thermoelectrics: From history, a window to the future," *Mater. Sci. Eng. R Reports*, vol. 138, no. July 2018, pp. 210–255, 2019.
- [8] L. D. Zhao, C. Chang, G. Tan, and M. G. Kanatzidis, "SnSe: A remarkable new thermoelectric material," *Energy and Environmental Science*, vol. 9, no. 10. Royal Society of Chemistry, pp. 3044–3060, 01-Oct-2016.
- [9] X. Zhang and L. D. Zhao, "Thermoelectric materials: Energy conversion between heat and electricity," *Journal of Materiomics*, vol. 1, no. 2. Chinese Ceramic Society, pp. 92–105, 01-Jun-2015.
- [10] S. Kasap, "Thermoelectric Effects in Metals," *Dep. Electr. Eng. Univ. Saskatchewan, Canada*, pp. 1–11, 2001.
- [11] Z. H. Dughaish, "Lead telluride as a thermoelectric material for thermoelectric power generation," *Phys. B Condens. Matter*, vol. 322, no. 1–2, pp. 205–223, Sep. 2002.
- [12] S. Cecchi, L. F. Llin, T. Etzelstorfer, and A. Samarelli, "Review of thermoelectric

- characterization techniques suitable for SiGe multilayer structures," *Eur. Phys. J. B* 2015 883, vol. 88, no. 3, pp. 1–8, Mar. 2015.
- [13] L. Yang, Z. G. Chen, G. Han, M. Hong, Y. Zou, and J. Zou, "High-performance thermoelectric Cu<sub>2</sub>Se nanoplates through nanostructure engineering," *Nano Energy*, vol. 16, pp. 367–374, Sep. 2015.
- [14] "Skutterudite: Mineral information, data and localities." [Online]. Available: <https://www.mindat.org/min-3682.html>. [Accessed: 18-Apr-2020].
- [15] M. Rull-Bravo, A. Moure, J. F. Fernández, and M. Martín-González, "Skutterudites as thermoelectric materials: Revisited," *RSC Advances*, vol. 5, no. 52, pp. 41653–41667, 2015.
- [16] A. Bhargava, "Wet Scrubbers – Design of Spray Tower to Control Air Pollutants Wet Scrubbers – Design of Spray Tower to Control Air," *Int. J. Environ. Plan. Dev.*, vol. 2, no. 1, pp. 68–73, 2016.
- [17] Clean Marine AS, "Information inquiry on wet scrubbers and TEG systems." 2020.
- [18] I. Klevtsov, A. Paist, and T. Bojarinova, "Aurukatla soojustehniline arvutus ja projekteerimine." TTÜ Energiatehnoloogia Instituut, 2007.
- [19] "Fluid property calculator." [Online]. Available: [https://web1.hszg.de/thermo\\_fpc/index.php](https://web1.hszg.de/thermo_fpc/index.php). [Accessed: 10-May-2020].
- [20] "Beca engineering." [Online]. Available: <http://www.beca-engineering.com/index.php>. [Accessed: 10-May-2020].
- [21] T. L. Bergman, A. S. Lavine, F. P. Incropera, and D. P. Dewitt, *Fundamentals of heat and mass transfer*, Seventh Ed. Don Fowley, 2011.
- [22] "Baltic Bolt." [Online]. Available: <https://balticbolt.ee/>. [Accessed: 15-May-2020].
- [23] A. Ots, *Soojustehnika aluskursus*. TTÜ Kirjastus, 2011.
- [24] *Water-tube boilers and auxiliary installations - Part 15: Acceptance tests: EVS-EN 12952-15:2003*. Estonian Centre for standardisation, 2003.
- [25] "WolframAlpha." [Online]. Available: <https://www.wolframalpha.com/input/>. [Accessed: 20-May-2020].

- [26] "Prevention of Air Pollution from Ships." [Online]. Available:  
[http://www.imo.org/en/OurWork/Environment/PollutionPrevention/AirPollution/  
Pages/Air-Pollution.aspx](http://www.imo.org/en/OurWork/Environment/PollutionPrevention/AirPollution/Pages/Air-Pollution.aspx). [Accessed: 24-May-2020].
- [27] W. K. Talley, *The Blackwell Companion to Maritime Economics*. Blackwell  
Publishing Ltd., 2012.



## APPENDICES

### Appendix 1 Exhaust gas average isobaric specific heat calculation

Equation for calculating average isobaric specific heat of exhaust gas [24].

$$c_p = (c_{pAd} + P_{1m}x_{H_2O} + P_{2m}x_{CO_2}) \times 1000, \quad (A1.1)$$

where  $c_{pAd}$  – the integral specific heat of dry air between 0 °C and t °C,  $J/(kg \cdot K)$ ,

$x_{H_2O}$  – water content in exhaust gas, kg/kg,

$x_{CO_2}$  – carbon dioxide content in exhaust gas, kg/kg.

$$c_{pAd} = a + \frac{b}{2}t + \frac{c}{3}t^2 + \frac{d}{4}t^3 + \frac{e}{5}t^4 + \frac{f}{6}t^5, \quad (A1.2)$$

where a, b, c, d, e and f – polynomial coefficients shown in Table A. 1,

t – temperature of exhaust gas, °C.

$$P_{1m} = a_1 + \frac{b_1}{2}t + \frac{c_1}{3}t^2 + \frac{d_1}{4}t^3 + \frac{e_1}{5}t^4, \quad (A1.3)$$

where  $a_1, b_1, c_1, d_1$  and  $e_1$  – polynomial coefficients shown in Table A. 1.

$$P_{2m} = a_2 + \frac{b_2}{2}t + \frac{c_2}{3}t^2 + \frac{d_2}{4}t^3 + \frac{e_2}{5}t^4, \quad (A1.4)$$

where  $a_2, b_2, c_2, d_2$  and  $e_2$  – polynomial coefficients shown in Table A. 1.

Table A. 1 Polynomial coefficients for equations (A1.2), (A1.3) and (A1.4)

| Polynom (A1.2) |              | Polynom (A1.3) |              | Polynom (A1.4) |              |
|----------------|--------------|----------------|--------------|----------------|--------------|
| a              | 1,004173     | a <sub>1</sub> | 0,8554535    | a <sub>2</sub> | -0,1002311   |
| b              | 1,91921E-05  | b <sub>1</sub> | 0,000203601  | b <sub>2</sub> | 0,000766186  |
| c              | 5,88348E-07  | c <sub>1</sub> | 4,58308E-07  | c <sub>2</sub> | -9,25962E-07 |
| d              | -7,01118E-10 | d <sub>1</sub> | -2,79808E-10 | d <sub>2</sub> | 5,2935E-10   |
| e              | 3,30953E-13  | e <sub>1</sub> | 5,63441E-14  | e <sub>2</sub> | -1,09357E-13 |
| f              | -5,67388E-17 |                |              |                |              |

## Appendix 2 Part list and prices of quenching segment

Table A.2 Part list and prices of quenching segment [17], [22]

| Part description               | Dimension                            | Material  | QTY<br>,pcs | Price, €/pcs | Price, €       |
|--------------------------------|--------------------------------------|-----------|-------------|--------------|----------------|
| <b>Shell</b>                   |                                      |           |             |              | <b>8052,96</b> |
| Plate                          | 16 mm x 1025 mm x 1025 mm            | EN 1.4404 | 4           | 603,01       | 2412,03        |
| Plate                          | 4 mm x 5999 mm x 1490 mm             | EN 1.4547 | 1           | 3518,20      | 3518,20        |
| Plate                          | 4 mm x 5999 mm x 899 mm              | EN 1.4547 | 1           | 2122,72      | 2122,72        |
| <b>Spray ring</b>              |                                      |           |             |              | <b>2261,51</b> |
| Pipe                           | NPS 3" 40s ASME B36.19 L=1745 mm     | EN 1.4410 | 2           | 225,56       | 451,13         |
| Pipe                           | NPS 2" 40s ASME B36.19 L=2031,5 mm   | EN 1.4410 | 4           | 159,92       | 639,68         |
| Pipe                           | NPS 2" 40s ASME B36.19 L=626,1 mm    | EN 1.4410 | 4           | 49,29        | 197,15         |
| End cap                        | NPS 3" 10s ASME B16.9                | EN 1.4410 | 2           | 23,65        | 47,29          |
| Spray nozzle                   | BETE 3/8" TF12 FCN                   | EN 1.4404 | 54          | 5,33         | 287,82         |
| Custom socket                  | 3/8" BSPP<br>Ø=25mm<br>L=28mm        | EN 1.4410 | 54          | 11,82        | 638,44         |
| <b>Additional spray nozzle</b> |                                      |           |             |              | <b>289,62</b>  |
| Plate                          | 4 mm x 106 mm x 79 mm                | EN 1.4410 | 16          | 2,15         | 34,40          |
| Pipe                           | NPS 1-1/2" 40s ASME B36.19 L=85,6 mm | EN 1.4410 | 8           | 3,97         | 31,78          |

Table A.2 continued

| <b>Part description</b>        | <b>Dimension</b>                          | <b>Material</b>             | <b>QTY<br/>,pcs</b> | <b>Price, €/pcs</b> | <b>Price, €</b> |
|--------------------------------|---|-----------------------------|---------------------|---------------------|-----------------|
| Pipe                           | NPS 1/2" 40s<br>ASME B36.19<br>L=488,9 mm | EN 1.4410                   | 8                   | 8,43                | 67,44           |
| Butt weld<br>connector         | HOKE CBW/ME<br>14mm 21,3mm                | EN 1.4401                   | 8                   | 5,40                | 43,20           |
| NaOH lance gasket              | 2mm                                       | KLINGER<br>Top-Chem<br>2005 | 8                   | 3,50                | 28,00           |
| Bolt                           | M16 x 40 DIN<br>931                       | A4-80                       | 16                  | 3,25                | 52,00           |
| Plain washer                   | M16 DIN 125A                              | A4-80                       | 16                  | 0,52                | 8,32            |
| Spring washer                  | M16 DIN 127                               | A4-80                       | 16                  | 0,65                | 10,40           |
| Nut                            | M16 DIN 934                               | A4-80                       | 16                  | 0,88                | 14,08           |
| <b>Stiffeners</b>              |   |                             |                     |                     | <b>1679,68</b>  |
| Plate                          | 8 mm x 2095<br>mm x 1048 mm               | EN 1.4404                   | 2                   | 630,07              | 1260,15         |
| Plate                          | 8 mm x 1192<br>mm x 90 mm                 | EN 1.4404                   | 1                   | 30,79               | 30,79           |
| Plate                          | 8 mm x 1175<br>mm x 90 mm                 | EN 1.4404                   | 2                   | 30,35               | 60,70           |
| Plate                          | 8 mm x 1153<br>mm x 90 mm                 | EN 1.4404                   | 1                   | 29,78               | 29,78           |
| Plate                          | 6 mm x 1624<br>mm x 40 mm                 | EN 1.4404                   | 16                  | 18,64               | 298,27          |
| <b>Supports</b>                |   |                             |                     |                     | <b>178,44</b>   |
| Zone 1 lance<br>support type 1 | 4 mm x 170 mm<br>x 452 mm                 | EN 1.4547                   | 6                   | 29,74               | 178,44          |
|                                |   |                             |                     | <b>Sum</b>          | <b>12462,20</b> |